Ni- and/or Mn-based Layered Transition Metal Oxides as Cathode Materials for Sodium Ion Batteries: Status, Challenges and Countermeasurements

Shenghan Wang[a], Chenglin Sun[a,*], Ning Wang[a,*]and Qichun Zhang[b*]

[a]*Key Laboratory of Physics and Technology for Advanced Batteries (Ministry of Education), College of physics, Jilin University, Changchun 130012, P. R. China*

[b]*School of Materials Science and Engineering, Nanyang Technological University, Singapore 639798.*

*Corresponding authors.

E-mail addresses: chengling@jlu.edu.cn (C. Sun), ningwang@jlu.edu.cn (N. Wang), qczhang@ntu.edu.sg (Q. Zhang)

Sodium ion batteries (SIBs) have been attracting great interests as alternatives for grid and mobile energy storage applications in modern world due to the enough natural abundance and low cost of sodium resources. To accelerate the practical application of SIBs system, the electrochemical performance of cathode materials should be further improved to satisfy the increasing worldwide demand. As promising cathode materials for SIB, layered transition metal oxides (LTMOs) exhibit high specific capacity and high energy density due to their appropriate voltage window. Here, recent progress and achievements of three representative LTMOs including Ni-based, Mn-based, and Ni/Mn co-based cathodes in terms of the relationship between structure design and electrochemical performance are summarized, aiming at cost reduction and performance improvement. The insights in this review focus on the development of LTMOs as cathodes for SIBs including overall battery performance, preparation strategies and operation mechanism, therefore speeding up the commercialization of SIBs.

Keywords:

Sodium ion batteries, Layered transition metal oxides, Cathodes, Structure design, Phase Transitions

1. Introduction

Rechargeable batteries are essential in our modern world due to their continuous electrical energy supplement in many areas.[1-5] In recent years, two main aspects have driven the development of rechargeable batteries: (1) the demand of powering mobile electronic devices including electric vehicles (EVs), notebook type personal computer (PC) and so on; and (2) the demand of building stationary grid electrical energy storage (EES) systems to integrate the renewable sources, which are intermittent and regional.[6,7] Apart from the frequently-used mobile phones and PCs, which cannot work without rechargeable batteries, both the hybrid EVs (which have stepped into global market) and the full EVs (which will be mass-produced in the near future) show great dependence on rechargeable batteries as well.[6,8-10] On the other hand, to alleviate the shortage of resource and reduce the environmental pollution, clean and renewable energy sources such as wind, solar, and tide, are widely applied to decrease the consume of conventional fossil fuels. Therefore, large-scale grids EES systems are urgently needed to store excess electrical energy of clean energy sources.[11-13]

Lithium ion batteries (LIBs) technology is a real successful story since its first commercialization in early 1990s by Sony. Due to their excellent battery performance and rapid growth, LIBs have been dominant in the market of portable electronics and electric vehicles from then on. Meanwhile, the reliance on LIBs will quickly rise with the realization of mass production of EVs. However, the limited Li resources in nature give rise to a concern about maintaining the stable supply chains of LIBs manufacturing industry.[14,15] Meanwhile the realistic cost of raw materials are increasing, for example, the price of lithium has tripled in the past decades. Therefore, LIBs system is hard to meet the increasing demand of market, letting alone supporting the expansion of grid EES systems which need a large amount of raw materials. From the view of sustainable development of EES devices, people need to find enough substitutes to address the problems caused by the shortage of lithium source. Sodium is, no doubt, a promising substitute for lithium due to its analogous chemical properties and large abundance.[16,17] Sodium ion batteries (SIBs) are promising

candidates for next-generation power sources because sodium sources are cheaper and of wide geographical distribution. Besides, Al is inactive with sodium, which can act as current collector of anode material instead of expensive Cu. As a result, SIBs might be more attractive than LIBs in large-scale grid storage, where the cost is more important than energy/power density of batteries. In addition, the ionic radius of sodium (1.02 Å) is larger than that of lithium (0.59 Å), which might bring lower desolvation energy in some organic solvents and smaller charge transfer resistance.[18] Therefore, it is believed that sodium should exhibit faster electrode kinetics than lithium.[19] With that in mind, SIBs are revisited in recent years.

Recent progresses in SIBs are remarkable since tremendous efforts have been devoted to this area.[9, 20-24] However, relatively poor electrochemical performance (including power/energy density, rate capability, reversible capacity, cycling stability etc.) of SIBs limits their commercialization both in mobile and stationary energy storage. Since cathode materials are an important part in the development of SIBs, it is very important to summary these materials and highlight the progress in this field. Among all cathode materials, layered transition metal oxides (LTMOs), polyanionic frameworks, and Prussian blue analogues (PBAs) have been widely demonstrated as promising candidate materials for SIBs. Especially in recent years, extensive researches have been carried out on these cathode materials for application in SIBs. Polyanionic compounds-based cathodes (such as phosphates, pyrophosphates, fluorophosphates, sulfates, *etc.*) are famous for their safety and long lifetime due to their stable chemical structure.[25-28] However, this kind of cathode materials are always accompanied with poor electrical conductivity and low specific capacity.[25,29,30] PBAs are another type of excellent cathode materials owing to their unique open framework, high theoretical capacity and low cost.[31,32] However, PBAs materials exhibited undesired rate capability and cycling stability in certain degree when they are used as cathodes of SIBs.[33] Comparing with the above-mentioned two cathode material systems, the outstanding merits of LTMOs cathodes are high capacity and facile synthesis although their cycling stability and air instability remain challenging.

LTMOs represent a large family consisting of 3d transition metal elements (from Ti to Cu) or their mixtures, thus providing large variety of potential options.[3,34] Therefore LTMO cathode materials have been strongly investigated.

In this review, recent progress in three kinds of LTMO cathode materials (including Ni-based, Mn-based and Ni/Mn co-based LTMOs) for application in SIBs are summarized. Specifically, this review will focus on the latest improvement of overall electrochemical properties including cycling stability, reversible capacity and rate capability, and the related structure revolution mechanism. The routes of structure design and structure-function-performance relationship of these cathode materials are discussed as well. Finally, the existed problems and further prospect of LTMOs as cathodes for SIBs are presented.

2. Structural strategies of LTMOs

Na_xTMO_2 ($0<x\leq1$, TM = V, Cr, Mn, Fe, Co, Ni), or LTMOs, are formed by the stacking of edge-sharing TMO_6 layers with the insertion of Na ion layers. This kind of materials is mainly classified as P2 type and O3 type structures. The letters “P” and “O” stand for the prismatic and octahedral sites being occupied by Na ions while 2 and 3 represent the numbers of oxygen stacking layers in one unit cell. As shown in Fig. 1a, the oxygen stacking styles of P2 type and O3 type structures are ABBA and ABCABC, respectively.[15] Besides, prime symbol (′) is usually used to denote structures with in-plane distortion of hexagonal lattice. Generally, the Na number “x” ranges between 0.6 and 0.7 in P2 type structure while changing between 0.7 and 1 in O3 type structure. For both P2 and O3 type materials, the extraction of Na^+ always leads to material phase transition, and some are irreversible. As a result, the corresponding chemical performance are affected. For P2 type structure, due to the gliding of TMO_2 sheets, new octahedral sites generate, and the initial phase turns to O2 type phase, where the oxygen stacking forms unique ABAC instead of the original ABBA as shown in Fig. 1a. For O3 type structure, when part of Na^+ extracts from O3 type structure, prismatic sites after the gliding of TMO_2 slabs and the oxygen stacking

changes from ABCABC to ABBCCA as shown in Fig. 1a. In some cases, the phase transition of O3 type will be more complicated. For example, O3 type $NaFe_{0.45}Co_{0.5}Mg_{0.05}O_2$ suffered from phase-transition process of O3-P3-P′3-O3′. Therefore, P2 type materials generally undergo simpler phase transition than O3 type materials and P2 type materials exhibit relatively-high cycling stability and rate capability. However, O3 type materials usually show high capacity because they involve larger amounts of Na ions than P2 type materials per unit.[3] To improve the electrochemical properties of LTMOs in SIBs in Fig. 1b, more concern should be given on how to suppress the irreversible phase transition and related structure revolution process. General method to reduce phase transition is to mix different transition metals together (e.g. V, Cr, Mn, Fe, Co, Ni) as well as using the cation substitution with Li^+, Cu^{2+}, Mg^{2+}, Zn^{2+}, Ti^{4+}, etc.

Although all of the 3d transition metal oxides have been demonstrated to show some activity in SIBs as sodium host, most of them are not suitable candidates for practical SIBs. Thus, by comparing the merits and drawbacks of six different transition metal-based oxides, single transition metal-based oxides (e.g. $NaVO_2$, $NaCrO_2$, $NaMnO_2$, $NaFeO_2$, $NaCoO_2$, and $NaNiO_2$) are chosen as the representative to discuss their specific capacity and feasibility. The theoretical specific capacities of $NaVO_2$, $NaCrO_2$, $NaMnO_2$, $NaFeO_2$, $NaCoO_2$, and $NaNiO_2$, are 253, 250, 243, 241, 235, and 235 mAh/g, respectively, where the difference is very small. However, in experiments, their measured capacities (120, 120, 197, 80, 40, and 123 mAh/g, respectively) are quite different from each other, where one can easily conclude that the specific capacity of transition metal oxides based on Mn and Ni are higher than others.[52,58,73,92,24,120] If feasibility is only taken into consideration, the V and Cr oxides would be first excluded due to their toxicity and high cost, and only other 4 materials left with reasonable performance: Mn is cost-effective although $NaMnO_2$ demonstrated high specific capacity. Fe-based LTMOs are famous for their low cost and high working voltage while Co-based $NaCoO_2$ shows high ionic diffusion. The most remarkable advantage of Ni-based LTMOs is its high working voltage. Based on

these discussions, most research groups believe that Ni and/or Mn-based LTMOs are ideal sodium host materials because these materials excellent specific capacity and high feasibility.

Although layered Na_xMnO_2 and Na_xNiO_2 are two widely-accepted cathode materials for SIBs due to the above-mentioned reasons, they still exhibit inevitable drawbacks. On one hand, Na_xMnO_2 system likely suffers from rapid capacity declining due to the strong Jahn-Teller distortion of Mn^{3+}.[35-37] Comparing with Mn^{2+} (d^5-type electron distribution with half-filled 5 electron orbits) and Mn^{4+} (d^3-type electron distribution with half-filled t_{2g} electron orbits), $Mn^{3+}[t_{2g}^3e_g^1]$ is prone to Jahn-Teller distortion due to the d4-type electron distribution without half-filled (or full-filled) electron orbit. On the other hand, Na_xNiO_2 system usually comes across irreversible complex structural evolution during charge/discharge cycling and large capacity loss during initial cycles.[38] To address this problems, the most direct and fundamental method is to integrate these two systems together as Ni/Mn-based LTMOs. Taking typical P2-$Na_x[Ni_{1/3}Mn_{2/3}]O_2$ as an example, the structural advantages (in aspect to single-based systems) could be well understood. According to theoretical simulation of P2-$Na_x[Ni_{1/3}Mn_{2/3}]O_2$, Ni ion experiences +2/+3/+4 transformation while Mn^{4+} remains same and being absent from redox reaction during charge/discharge process.[39,40] According to the density of state (DOS) calculation of P2-$Na_x[Ni_{1/3}Mn_{2/3}]O_2$, 3d orbitals ($t_{2g}$ and e_g orbitals) of Ni ions or Mn ions experience different electron transition. When x=2/3 in P2-$Na_x[Ni_{1/3}Mn_{2/3}]O_2$, t_{2g} orbitals are fully occupied while the energy levels of spin-up states in the e_g orbitals is empty, resulting in $t_{2g}^6e_g^2$ electron configuration. Here Ni ion exists as Ni^{2+}. When half of Na^+ extracts (x=1/3), the electron configuration turns to $t_{2g}^6e_g^1$ because full of t_{2g} orbitals and one of the spin-down e_g orbitals are occupied. Accordingly, Ni ion turns to trivalent. When Na^+ is fully extracted, most of electrons in e_g energy level are removed, resulting in the formation of nearly Ni^{4+}. Meanwhile, Mn ions remain at tetravalent with fully occupied t_{2g} orbitals and completely empty e_g orbitals during Na^+ extraction. As a result, Jahn-Teller inactive Mn ion maintains the structural

integrity while Ni ion provides a wide voltage window during redox reaction. The Ni/Mn-based LTMOs show high specific capacity and high structure stability. The illustration of the corresponding process is shown in Fig. 1c. Besides the DOS calculation, another calculation through nudged elastic band (NEB) method indicates that the required energy of Na^+ diffusion in P2-$Na_x[Ni_{1/3}Mn_{2/3}]O_2$ is only 170 meV ($1/3<x<2/3$), which is lower than the Li^+ analogues. In addition to NEB method, the chemical diffusion coefficient of Na^+ was also calculated to be as high as 7×10^{-9}-1×10^{-10} cm^2s^{-1} ($1/3<x<2/3$) under galvanostatic intermittent titration technique (GITT) calculation.[40] Accordingly, both NEB and GITT methods demonstrate the high diffusivity of Na ions in Ni/Mn-based LTMOs system, leading to high rate performance as cathode materials for SIBs. A large amount of sodium ions in half cells and full cells based on Ni/Mn LTMOs cathodes exhibit the satisfied overall battery performance, which are summarized as following, and some of them are shown in Fig. 2 and Table 1.

In summary, the binary system not only inherits the advantages of both Na_xMnO_2 and Na_xNiO_2 system (Mn^{4+} stabilizes the structure by inhabiting the Jahn-Teller effect of Mn^{3+} while Ni^{2+}/Ni^{3+}/Ni^{4+} takes full advantage of its wide working voltage), but also exhibits high Na^+ mobility, high specific capacity and high structure stability during cycling. On the basis of the direct combination of Ni and Mn in one system, other effective methods (including cation substituting, nano-sizing, carbonaceous compositing et al) are widely investigated to further improve the feasibility and overall energy storage ability. The detailed progress on different Ni- and/or Mn-based LTMOs as cathode materials for SIBs are reviewed as following.

3. Mn-based LTMOs

3.1 Mn-based single LTMOs

Na_xMnO_2-type cathode materials hold great application potential due to their relative abundance and low cost.[41-44] This kind of layered materials are always distributed at the stoichiometry x>0.5, among which P2-type Na_xMnO_2 cathode materials are the most extensively investigated system on the account of previous reports.[45-48] However, the strong Jahn-Teller effect of Mn^{3+} always leads to the sharp decline of capacities after several charge/discharge circles. To enhance the cycling stability, researchers usually regulate the Jahn-Teller effect by new structure design and/or substituting other inactive cations. As an example of regulating Jahn-Teller effect, Komaba and co-workers developed a single-phase route to fabricate distorted P2-$Na_{2/3}MnO_2$ with the capacity of 216 mAh g^{-1}, the average voltage window at 3 V and the energy density of 590 Wh kg^{-1} in a non-aqueous Na cell as well as excellent cycle stability.[36] Such a cell performance is very promising for practical applications. The improved electrochemical performance was due to the co-operative Jahn-Teller distortion of six-coordinated Mn^{III} (t_{2g}^3-e_g^1).

Cation substitution methods involving lithium, magnesium, aluminum, and copper are frequently employed to suppress Jahn-Teller distortion in Mn-based LTMOs by affecting the electron orbitals of Mn. This method is found to stabilize the lattice structure and maintain the electrochemical properties of P2-type Na_xMnO_2 cathode materials.[49-56] Li-substituted P2-$Na_{0.6}Li_{0.2}Mn_{0.8}O_2$ delivered a high specific capacity up to 190 mAh g^{-1} after 100 cycles between 2.0-4.6 V versus Na/Na^+ in Fig. 3a.[49] The addition of lithium improved structural stability by restraining the phase transition process and reducing the Jahn-Teller distortion.[50] Meanwhile, the charge/discharge processes are accompanied with an activation process based on the extraction of Li^+. The substitution of Mn with Mg in P2-type Na_xMnO_2 also leads to smooth electrochemical profiles, an enhanced Na-ion conduction, and a high reversible capacity.[52,57,58] Grey and co-workers compared the structure evolution of the layered framework upon electrochemical cycling of three different $Na_xMn_{1-y}Mg_yO_2$ (y = 0.0, 0.05, 0.10) compositions, and they found that the 5% Mg-doped compound exhibited a relatively high rate capability and excellent structural stability in Fig. 3b and c.[54] Besides cation substitution, nano-compositing is frequently used to produce Mn-based cathode materials. For example, Xia group reported P2-type $Na_{0.7}MnO_{2.05}$ nanotube/carbon nanotube (NMO/CNT) core/branch composites in Fig. 3d and e.[59] The addition of CNT cocoon-like branches improved

the migration of electrons and stabilized the lattice structure during Na^+ insertion/ extraction processes. Therefore, the NMO/CNT material showed improved cell performance with capacity retention of 88% at 0.1 A g^{-1} after 100 cycles in Fig. 3f. Full cell test with NMO/CNT as a cathode material also exhibited a large capacity retention of 71% after 200 cycles at 100 mA g^{-1} and superior rate performance with a helical carbon nanofiber anode. This inspired structure design strategy is meaningful for the development of cathode materials for SIBs.

Mn/Fe-based layered oxide cathodes are also attractive due to their cost-effectiveness, natural abundance and non-toxicity, accompanied with high working voltage of Fe^{3+}/Fe^{4+}. The partial substitution of Mn with Fe could raise the average working voltage and suppress the Jahn-Teller distortion at the same time.[60] The stoichiometry of iron and manganese could influence the phase of materials.[61] In this system, $Na_xMn_yFe_{1-y}O_2$ cathode showed the best electrochemical performance at y=0.5.[42] Komaba and co-workers synthesized both P2-$Na_{2/3}[Fe_{1/2}Mn_{1/2}]O_2$ and O3-$Na[Fe_{1/2}Mn_{1/2}]O_2$ materials with enhanced reversible capacity and energy density.[44] P2-$Na_{2/3}[Fe_{1/2}Mn_{1/2}]O_2$ delivered up to 190 mAh g^{-1} with an average voltage of 2.75 V versus Na^+/Na, which is higher than that of O3-$Na[Fe_{1/2}Mn_{1/2}]O_2$ in Fig. 3g and h due to the formation of highly reversible OP4 phase when charged over 4.2 V. The energy density of P2-$Na_{2/3}[Fe_{1/2}Mn_{1/2}]O_2$ was estimated to 520 mWh g^{-1}, which is comparable with the commercially available $LiFePO_4$ (about 530 mWh g^{-1} versus Li/Li^+). Meanwhile, the density of P2-$Na_{2/3}[Fe_{1/2}Mn_{1/2}]O_2$ (about 4.1 g cm^{-3}) is higher than that of $LiFePO_4$ (about 3.6 g cm^{-3}). The increased energy density can contribute to the cost reduction indirectly. Based on the above-mentioned advantages, P2-$Na_{2/3}[Fe_{1/2}Mn_{1/2}]O_2$ holds great potential to be applied in large scale SIBs. Through the use of *in situ* Raman and XRD measurements, a reversible phase transition of P2-OP4 can be confirmed to only happen between 4.0 V and 4.2 V.[62]

Rojo group synthesized both P2-$Na_{2/3}Fe_{2/3}Mn_{1/3}O_2$ and O3-$Na_{2/3}Fe_{2/3}Mn_{1/3}O_2$ materials with excellent electrochemical properties and gave a direct comparison of the electrochemical performance between the two polymorphs with an identical Fe-Mn stoichiometry for the first time.[41] The reversible capacity of both phases stayed

at 120 mA h g^{-1} after 15 cycles, with average voltages of 2.50 V and 2.74 V and corresponding energy densities of 386.05 Wh kg^{-1} and 423.87 Wh kg^{-1} for P2-$Na_{2/3}Fe_{2/3}Mn_{1/3}O_2$ and O3-$Na_{2/3}Fe_{2/3}Mn_{1/3}O_2$ as shown in Fig. 4a and b. These results clearly indicate that both P2 and O3 phases $Na_{2/3}Fe_{2/3}Mn_{1/3}O_2$ exhibited nearly the same electrochemical performance as cathode materials in SIBs. To further increase the reversible capacity of SIBs, NaN_3 as a sacrificial salt was added into full cell with $Na_{0.67}[Fe_{0.5}Mn_{0.5}]O_2$ as cathode and hard carbon as anode.[63] The reversible capacity increased from 50 mAh g^{-1} for 0% wt NaN_3 to ~130 mAh g^{-1} for 20% wt NaN_3. However, the reversible capacity would decrease when the amount of NaN_3 further increased.

Other cations-doped Mn/Fe-based layered oxide cathodes, such as Cu-doped P2-$Na_{7/9}Cu_{2/9}Fe_{1/9}Mn_{2/3}O_2$, O3-$Na_{0.9}[Cu_{0.22}Fe_{0.30}Mn_{0.48}]O_2$ and Ti-doped P2-$Na_{2/3}Mn_{0.8}Fe_{0.1}Ti_{0.1}O_2$ also exhibited advanced electrochemical performance.[64-66] Gu and co-workers designed an air-stable P2-$Na_{7/9}Cu_{2/9}Fe_{1/9}Mn_{2/3}O_2$ with high Na content, which exhibited excellent electrochemical performance both in half cell and in full cell (coupled with hard carbon) as shown in Fig. 4c and d.[65] Hu et al prepared air-stable O3-$Na_{0.9}[Cu_{0.22}Fe_{0.30}Mn_{0.48}]O_2$ cathode material, which displayed excellent cycling stability and rate performance by using 3.2 V class battery with hard carbon anode in Fig. 4e and f. The addition of copper may be helpful to the improvement of air stability of LTMOs based on two aspects: first, Cu ion has the ability to improve the average storage voltage to prevent the oxidization from water/oxygen/CO_2; second, Cu may help to form new surface structures and compositions to avoid direct contact with air.[66] Recently, biphasic P2/O3-$Na_{2/3}Li_{0.18}(Mn_{0.8}Fe_{0.2})O_2$ material was synthesized by a facile solid-state reaction.[67] This cathode material delivered an initial discharge capacity of 125 mAh g^{-1} and 105 mAh g^{-1} at C/10 and 1C rates respectively, within 1.5-4.2V versus Na^+/Na as shown in Fig. 4g and h. In fact, O3 phase barely changed its structure during charge/discharge cycles based on the *ex situ* XRD studies. Therefore, the role of O3 phase was to stabilize the lattice structure by reducing the gliding of main phase. The post ball milling treatment can enhance the reversible capacity and energy density comparing to the pristine materials (Fig. 4i). For Mn/Fe-based binary LTMOs, the remaining challenges lie in improving cycling stability and reducing Jahn-Teller distortion by proper cation substitution and biphasic

structure design.

3.2 Mn/Co-based binary and Mn/Fe/Co-based ternary LTMOs

Cobalt is a common substitution element in LTMOs. For example, stable P2 phase structure can be obtained by partial substitution of Mn with cobalt in P′2-$Na_{2/3}MnO_2$.[68] Yamada *et al* synthesized a series of P2-$Na_{2/3}Mn_yCo_{1-y}O_2$ compounds (y= 0, 1/6, 1/3, 1/2, 2/3, 5/6, and 1) by one-step solid-state reaction. The substitution amount of Co in P2-$Na_{2/3}Mn_yCo_{1-y}O_2$ had strong influence on the valence states. From the charge-discharge curves at 30 mA g^{-1}, the redox potential of Co^{4+}/Co^{3+} and Mn^{4+}/Mn^{3+} shifted systematically by changing the ratio of Co/Mn. They also found that the initial specific capacity increased while the cycling stability declined with the increase of y.[69] It is found that a small amount of Co substitution in P2-Na_xMnO2 could lead to P2-$Na_xCo_{0.1}Mn_{0.9}O_2$ with improved specific capacity and cycling stability.[70] The addition of cobalt (*ca.* 10%) can suppress the Jahn-Teller effect, promote the intercalation of Na^+ and enhance the conductivity of Na^+.[71]

When the substitution amount of Co increases to *ca*. 50%, the corresponding voltage profile became smoother instead of multiple plateaus accompanied by great electrochemical performance. P2-$NaCo_{0.5}Mn_{0.5}O_2$ delivered 124.3 mAh g^{-1} in first discharge at 10C with 97% capacity retention after 30 cycles and 80 mAh g^{-1} in first discharge at 5C, with 99% capacity retention after 100 cycles.[72] Another homologous material P2-$Na_{0.67}Co_{0.5}Mn_{0.5}O_2$ demonstrated a higher discharge capacity of 147 mAh g^{-1} within the voltage between 1.5 V and 4.3 V *versus* Na^+/Na due to the reversible insertion/de-insertion of 0.56 mole Na^+ in Fig. 5a.[73] This material also showed excellent cyclic stability even at high C rate with 0.026% capacity decline per cycle over 2000 cycles at 30 C (Fig. 5b). P2-$Na_{0.67}Co_{0.5}Mn_{0.5}O_2$ exhibited no phase transition during charge/discharge cycling between 1.5V and 4.3 V according to *in situ* XRD measurement. It was found that further increasing the stoichiometry of Co substitution such as P2-$Na_{2/3}Co_{2/3}Mn_{1/3}O_2$ and P2-$Na_xCo_{0.7}Mn_{0.3}O_2$ could lead to the obvious plateaus in voltage profile during charge/discharge cycles. Nevertheless, the P2-$Na_{2/3}Co_{2/3}Mn_{1/3}O_2$ exhibited good reversibility for more than 0.5 mole Na^+

intercalation between 1.5 V and 4.0 V while the P2-$Na_xCo_{0.7}Mn_{0.3}O_2$ had excellent cycle capability with 84% capacity retention after 225 cycles at 1C rate and 75% of at a 30 C (compared to 1 C cycling) (Fig. 5c and d).[74,75]

Cobalt substitution in Mn-based cathode materials can lead to high voltage capacity and rate capability, although this method always brings multiple plateaus in voltage profile and declines in whole capacity. However, most of the Mn-Co based cathode materials are unstable in air. Furthermore, taking consideration of high cost and toxicity, there is still a long way to achieve practical application for this material system.

For substituting Mn with both Fe and Co in Na_xMnO_2, Jung and co-workers investigated the electrochemical performance of a series of P2-$Na_{0.7}[(Fe_{0.5}Mn_{0.5})_{1-x}Co_x]O_2$ (x=0, 0.05, 0.10, and 0.20) during charge/discharge cycling in Fig. 5e and f.[76] The P2-$Na_{0.7}Fe_{0.4}Mn_{0.4}Co_{0.2}O_2$ suffered from about 15% volume expansion during desodiation due to phase transition from P2 to O2 after a plateau at ≈4.1 V and ineluctable TMO_2 slabs gliding. This large volume change during desodiation/sodiation can lead to the gradual capacity loss after continuous cycling. In attempt to suppress phase transition, Ceder and co-workers prepared the new type P2-$Na_{2/3}(Mn_{1/2}Fe_{1/4}Co_{1/4})O_2$, which exhibited a decent rate capability in Fig. 5g and h due to the wide region of single P2 phase with low Na^+ diffusion and short range ordering of Na^+ during desodiation processes. Based on these merits, P2-$Na_{2/3}(Mn_{1/2}Fe_{1/4}Co_{1/4})O_2$ has been considered as a promising cathode candidate for high-power batteries.[77] P2-$Na_{2/3}Mn_{1/3}Fe_{1/3}Co_{1/3}O_2$ cathode material was also demonstrated to show a stable cycling performance under a 4.1V cutoff voltage.[78]

4. Ni-based LTMOs

4.1 Ni-based single LTMOs

Compared with Mn-based cathode materials, significant progress in Ni-based LTMOs have also been made in SIBs during the past few years.[79] Rojo and

co-workers reported that monoclinic O′3-$NaNiO_2$ suffered from irreversible capacity decline due to several phase transitions including O′3-, P′3-, P″3-, O″3-, and O‴3 during Na^+ charging/discharging cycles and strong Jahn-Teller distortion of Ni^{3+}, resulting in initial capacity loss.[38] In this content, $Na_3Ni_2MO_6$ (M=Sb^{5+}, Bi^{5+}, *etc.*)-type materials were developed with a honeycomb layered superstructure. Sb-based honeycomb layered O′3-$Na_3Ni_2SbO_6$ demonstrated excellent cycling stability and high-C rate in Fig. 6a and b.[80] O′3-$Na_3Ni_2SbO_6$ exhibited a full theoretical discharge capacity of 130 mAh g^{-1}.[81] Recently, Nam et al reported Bi-based O′3-$Na_3Ni_2BiO_6$ with a honeycomb-layered structure.[82] In the honeycomb structure, each BiO_6 octahedron was surrounded by six NiO_6 octahedron to take full advantage of $Ni^{2+}/Ni^{3+}/Ni^{4+}$ redox reaction. Bi^{5+} can keep the structure integrity absent in the electrochemical reaction. During charge/discharge cycles, the O′3 phase transformed into P′3 phase during the first voltage plateau at 3.25 V, then to O1 phase during the second voltage plateau at 3.5 V according to *in situ* XRD measurement. Since the above-mentioned fully-reversible phase transitions led to only 1% volume change, the O′3-$Na_3Ni_2BiO_6$ showed high cycling stability. As a result, honeycomb layered O′3-$Na_3Ni_2BiO_6$ cathode delivered 106 mAh g^{-1} discharge capacity with slight capacity loss over 50 cycles as shown in Fig. 6c and d. The Ni-based LTMOs with a honeycomb structure is no doubt a new route to develop efficient cathode materials for SIBs. Further work should be focused on improving cell performance accompanied by cost reduction.

Ti substitution is a widely-accepted route to improve electrochemical properties, especially for cycling stability of Ni-based LTMOs cathode materials. By attempting different stoichiometry ratios, O3-$NaNi_{0.5}Ti_{0.5}O_2$ and $Na_{0.8}Ni_{0.4}Ti_{0.6}O_2$ were well developed.[83-86] Among which, $Na_{0.8}Ni_{0.4}Ti_{0.6}O_2$ delivered 85 mAh g^{-1} reversible discharge capacity with 75% capacity retention over 150 cycles as shown in Fig. 6e-g. Finally, the Ni-based LTMOs cathode materials demonstrated high reversible capacity and cycling stability.

4.2 Ni/Co- and Ni/Fe-based binary LTMOs

The partial substitution of Ni with Fe and/or Co has been widely employed to suppress Jahn-Teller distortion in Ni-based LTMOs. Mixing different transition metals in different ratios always lead to different phase transition involving different redox processes of cathode materials during cycling. O3-$NaFe_{0.5}Ni_{0.54}O_2$ and $NaFe_{0.3}Ni_{0.7}O_2$ provided the reversible capacity of 112 and 135 mAh g^{-1} with initial coulombic efficiencies of 89% and 93%, respectively.[87] Kim et al compared the electrochemical properties and the structural evolution during Na^+ insertion/extraction process of O3-$NaNi_{0.5}Co_{0.5}O_2$ and $NaNi_{0.5}Fe_{0.5}O_2$.[88] O3-$NaNi_{0.5}Co_{0.5}O_2$ delivered higher reversible capacity in a broader voltage window between 2 and 4.2 V than O3-$NaNi_{0.5}Fe_{0.5}O_2$, where the voltage window was limited to 2-3.9 V. The capacity of O3-$NaNi_{0.5}Fe_{0.5}O_2$ declined during 3.9-4.2V due to the migration of Fe^{4+}, leading to the irreversible structure change. Based on the *in situ* XRD results and voltage profile of discharging process, O3-$NaNi_{0.5}Co_{0.5}O_2$ showed complicated phase transitions including three different O3 and three different P3 phases resulting in several plateaus while O3-$NaNi_{0.5}Fe_{0.5}O_2$ exhibited only O3-P3 phase transition with smooth voltage profiles in Fig. 7a and b.

The Ni/Fe/Co-based ternary cathode material O3-type $NaNi_{1/3}Co_{1/3}Fe_{1/3}O_2$ demonstrated high reversible capacity, rate capability and energy density. It delivered a reversible capacity of ~165 mAh g^{-1} with an energy density of ~500 Wh kg^{-1} at C/20.[89] Ti-doping in this system can lower average valence state of Fe, Co or Ni, resulting in the improvement of battery performance and structure stability. For example, $NaFe_x(Ni_{0.5}Ti_{0.5})_{1-x}O_2$ (x = 0.2 and 0.4) cathode delivered an initial discharge capacity of 120 mAh g^{-1} at 12 mA g^{-1} in a narrow voltage window of 3.75-2.60 V.[90] O3-$Na[Fe_{1/3}Ni_{1/3}Ti_{1/3}]O_2$ and $NaNi_{1/4}Co_{1/4}Fe_{1/4}Ti_{1/4}O_2$ were also reported.[91,92] O3-$Na[Fe_{1/3}Ni_{1/3}Ti_{1/3}]O_2$ cathode materials demonstrated high discharge capacities, good rate capability and cycling performance as well as good safety properties in Fig. 7c and d. The main redox reaction is based on nickel ions instead of iron ions while the titanium ions help to maintain the structural stability.[91] $NaNi_{1/4}Co_{1/4}Fe_{1/4}Ti_{1/4}O_2$ also exhibited long cycling life as shown in Fig. 7e.[92] The

ratio of different transition metal elements in the layered oxide cathode materials should be further optimized to improve electrochemical properties and structural stability of the as-prepared materials.

5. Mn/Ni-based LTMOs

5.1 Mn/Ni-based binary LTMOs

Among numerous LTMOs, Mn/Ni-based binary LTMOs arouse the most interest as cathode materials for SIBs. This system is found to demonstrate wide voltage window based on the $Ni^{2+}/Ni^{3+}/Ni^{4+}$ redox reaction while the structural stability can be maintained due to the inactive Mn^{4+}. The variety of Mn/Ni-based LTMOs including P2-type, O3-type and P2/O3 type biphasic LTMOs, can be produced through different kinds of substitution elements and blend ratios.

$Na_{2/3}Ni_{1/3}Mn_{2/3}O_2$ is a typical P2 type Mn/Ni-based binary LTMOs, delivering as high as 160 mAh g^{-1} reversible capacity between 2.0-4.5 V operating voltage.[39] However, there was a long plateau over 4.2 V resulting in 20% volume change and capacity fading. This phenomenon was mainly due to the irreversible P2-O2 phase transition. Effective methods including appropriate control of element ratio and electrochemically inactive cation substitution of partial Ni have been attempted to suppress phase transition and stabilize lattice structure at high cutoff voltage. Meng and co-workers developed Na-excess P2-$Na_{0.78}Ni_{0.23}Mn_{0.69}O_2$ cathode material, which delivered a reversible first cycle capacity of 138 mAh g^{-1} at 0.1 C within 2.0-4.5 V and still provided a high reversible capacity of 120 mAh g^{-1} at 5 C.[93] The cycling stability of P2-$Na_{0.78}Ni_{0.23}Mn_{0.69}O_2$ is outstanding over a wide voltage window by reducing the P2-O2 phase transition upon cycling to 4.5 V. They also evidenced the existence of oxygen vacancies in LTMOs for the first time.

Cation substitution is also widely used to stabilize structure and improve cycling performance by suppressing the P2-O2 phase transition. Among a series of

Mg-substituted P2-$Na_{0.67}Mn_{0.67}Ni_{0.33-x}Mg_xO_2$ ($0 \leq x \leq 0.33$), $Na_{0.67}Mn_{0.67}Ni_{0.28}Mg_{0.05}O_2$ can deliver up to 123 mAh g^{-1} with 3.7 V average discharge voltage versus Na^+/Na, resulting in a high energy density of 445 Wh kg^{-1} as cathode material for SIB (in Fig. 8a and b).[94] Based on *ex situ* XRD results, the P2-O2 phase transition of $Na_{0.67}Mn_{0.67}Ni_{0.28}Mg_{0.05}O_2$ was reduced compared to the $Na_{0.67}Mn_{0.67}Ni_{0.33}O_2$ material. The existence of inactive Mg^{2+} retained more Na^+ in the prismatic sites resulting in highly structural integrity during charging process. Therefore, the charge/discharge processes were limited to only a single-phase reaction, resulting in enhanced cycling performance. $Na_{0.67}Mn_{0.8}Ni_{0.1}Mg_{0.1}O_2$ was also prepared with high rate capability and cycling stability during charge/discharge processes due to the improved *d*-spacing of the Na-ion diffusion layer.[57]

It was found that Li doping could keep high Na content in interlayer space at all stages of charging and reduce the gliding of TMO_2 layer and water uptake. As a result, the Li-substituted P2-$Na_{0.8}Li_{0.12}Ni_{0.22}Mn_{0.66}O_2$ cathode exhibited a smoother voltage profile and better rate performance than P2-$Na_{2/3}Ni_{1/3}Mn_{2/3}O_2$ in Fig. 8c and d.[95] P2-$Na_{0.8}Li_{0.12}Ni_{0.22}Mn_{0.66}O_2$ demonstrated high reversible cycling performance in a wide voltage window because Li-substitution can stabilize structure by delaying the P2-O2 phase transition to as high as 4.4 V.[96] Water intercalation was also observed over 3.7 V charge for $Na_xNi_{1/3}Mn_{2/3}O_2$, but for $Na_xLi_{0.12}Ni_{0.22}Mn_{0.66}O_2$, water uptake happened at 4.4 V confirmed by ^{23}Na solid-state nuclear magnetic resonance (NMR).[39,40] Cao and coworkers reported Cu-substituted P2-type $Na_{0.67}Ni_{0.1}Cu_{0.2}Mn_{0.7}O_2$ as a high performance cathode material for SIB.[97] The substitution of Cu improved the cycling stability by preventing the P2-O2 phase transition. Different from other electrochemical inactive cations, Cu substitution can improve the rechargeable capacity because Cu^{2+}/Cu^{3+} redox reaction was electrochemical active during charge/discharge cycles.[98]

The effects of other cations (Zn, Al, Ti etc) substitution in P2 type Ni/Mn-based binary LTMOs were also investigated. For example, $Na_{0.66}Ni_{0.33-x}Zn_xMn_{0.67}O_2$, $Na_{2/3}Ni_{1/3}Mn_{5/9}Al_{1/9}O_2$, and $Na_{2/3}[Ni_{1/3}Mn_{1/2}Ti_{1/6}]O_2$ exhibited improved battery

performance by suppressing phase transition during Na^+ insertion/extraction.[99-101]

Recently, Liu et al introduced Al_2O_3-coated $Na_{2/3}[Ni_{1/3}Mn_{2/3}]O_2$ as a cathode material with a thickness <12 nm.[102] The surface Al_2O_3 layers could suppress unfavorable side reactions at high voltage, resulting in improved cycling stability and rate performance compared with the non-coated $Na_{2/3}[Ni_{1/3}Mn_{2/3}]O_2$ material as displayed in Fig. 8e and f. It was also reported that the coated Al_2O_3 nanolayers on the surface of $Na_{2/3}[Ni_{1/3}Mn_{2/3}]O_2$ enhanced the kinetics of Na^+ diffusion by promoting the decomposition of the salt in electrolyte and delayed the degradation of the active materials.[103] Similarly, Myung and co-workers coated an conductive $NaPO_3$ nanolayer (about 10 nm) on the surface of P2 $Na_{2/3}[Ni_{1/3}Mn_{2/3}]O_2$ to avoid the exposure of cathode material to HF and H_2O in the electrolyte.[104] As a result, the full cell based on $NaPO_3$-coated $Na_{2/3}[Ni_{1/3}Mn_{2/3}]O_2$/hard carbon showed an improved cycling stability with 73% capacity retention after 300 cycles compared to non-coated sample (Fig. 8g and h). The surface $NaPO_3$ nanolayers also suppressed the formation of byproducts on the surface of cathodes, thus decreasing the cell resistance.

Except for P2-type, O3-$Na[Ni_{1/2}Mn_{1/2}]O_2$ has also been studied. O3-$Na[Ni_{1/2}Mn_{1/2}]O_2$, consists of Ni^{2+} and Mn^{4+}, delivered a reversible capacity of 125 mAh g^{-1} when cycled at a current density of 4.8 mA g^{-1} in the voltage range of 2.2-3.8V, accompanied with complex phase transition of O3hex.-O′3mon.-P3hex.-P′3mon.-P3″hex during charge/discharge cycling.[105-107] Only 5% of initial capacity can be retained after 50 cycles, resulting in poor rate performance in high voltage region. To address this problem, partial substitution of Mn^{4+} with Ti^{4+} can enhance the interslab distance and suppress irreversible structure transformation. Guo group synthesized a series of O3-$NaNi_{0.5}Mn_{0.5-x}Ti_xO_2$ materials, among which, $NaNi_{0.5}Mn_{0.2}Ti_{0.3}O_2$ delivered 135 mAh g^{-1} with 85 % capacity retention at 1 C after 200 cycles based on the Ni^{2+}/Ni^{3+} redox couple (Fig. 9a).[108] Partial Ti substitution suppressed irreversible multiple phase transition in high voltage region during Na^+ insertion/extraction process (Fig. 9b).

Li substitution in O3-type materials could improve battery performance but brought

Li^+ loss due to the migration of Li^+ into Na^+ layers during Na^+ deintercalation/intercalation. A Cu/Ti co-based $NaNi_{0.45}Cu_{0.05}Mn_{0.4}Ti_{0.1}O_2$ was reported with an improved electrochemical performance and air stability in Fig. 9c and d.[109] Recently, O3-type $Na[Li_{0.05}Mn_{0.50}Ni_{0.30}Cu_{0.10}Mg_{0.05}]O_2$ was synthesized via an industrially feasible coprecipitation method, followed by thermal treatment.[110] Based on the unique nano-crystal aggregated microsphere architecture, the as-prepared O3-$Na[Li_{0.05}Mn_{0.50}Ni_{0.30}Cu_{0.10}Mg_{0.05}]O_2$ delivered a high reversible capacity of 172 mA h g^{-1} at 0.1 C and excellent capacity retention of 70.4% after 1000 cycles at 20 C. High energy density up to 215 Wh kg^{-1} demonstrated its high possibility to be employed in practical SIBs for large scale electrical energy storage. P2/O3 $Na_{0.7}Li_{0.3}Ni_{0.5}Mn_{0.5}O_{2+d}$ delivered 125 mAh g^{-1} at 15 mA g^{-1} between 2.0-4.05 V and retained 95% of initial capacity over 20 cycles, but suffered from multiple phase transitions as shown in Fig. 9e and f.[111]

5.2 Ni/Mn/Co-based ternary LTMOs

In Liu research, they found that Co^{3+} substitution can enhance electronic conductivity during charge/discharge cycling, and lead to a higher rate capability.[112] P2-$Na_xNi_{0.22}Co_{0.11}Mn_{0.66}O_2$ exhibited a low initial capacity of 117 mAh g^{-1} with average discharge voltage of 3.3 V versus Na^+/Na, but good rate capability for 200 cycles.[113] Other congeneric materials (e.g. P2-$Na_{2/3}Co_{2/3}Mn_{2/9}Ni_{1/9}O_2$, $Na_{0.67}[Ni_{0.4}Co_{0.2}Mn_{0.4}]O_2$, $Na_xMn_{2/3}Co_{1/6}Ni_{1/6}O_2$, and P2-$Na_xMn_{0.60}Ni_{0.30}Co_{0.10}O_2$[114-117]) with different element ratios were also reported. This type of P2-type materials suffered from rapid capacity decay in high voltage regions due to P2-O2 phase transition. Therefore, reversible cycles were limited under 4.0 V. Apart from P2-type materials, O3-type $Na[Ni_xCo_yMn_z]O_2$ (x= 1/3, 0.5, 0.6, and 0.8) were also attempted to be applied as cathodes for SIBs application. Among these materials, $NaNi_{1/3}Co_{1/3}Mn_{1/3}O_2$ exhibited an improved reversible capacity and high rate capability. [118,119] Based on the first-principle calculation, the average valence states of nickel, cobalt, and manganese elements were +2, +3, and +4, respectively. Therefore, the full use of Ni^{2+}/Ni^{3+}, Ni^{3+}/Ni^{4+}, Co^{3+}/Co^{4+} redox couples can provide

high specific capacity while the inactive Mn^{4+} is beneficial for the structure stability.[120]

By introducing electrochemical inactive Al ion into this system, capacity retention increased. The as-prepared P2-$Na_{0.67}[Mn_{0.65}Ni_{0.15}Co_{0.15}Al_{0.05}]O_2$ microflakes as cathodes delivered a reversible capacity of 123 mAh g^{-1} and retained 95.4% capacity over 50 cycles.[121-122] In addition to cation substitution, the synthesis of composite materials were also applied to optimize the battery performance of these LTMOs. Al_2O_3-coated P2-$Na_{2/3}(Mn_{0.54}Ni_{0.13}Co_{0.13})O_2$ showed an excellent cycling stability, especially in high voltage regions delivering a reversible capacity of 121 mA h g^{-1} within 2-4.5V at 1C.[123] Likewise, $Na_{2/3}[Mn_{0.55}Ni_{0.30}Co_{0.15}]O_2$ composited with multi-walled carbon nanotubes cathode materials exhibited high electrochemical performance and rate capability because carbon nanotubes provided more paths for Na^+ transportation.[124]

5.3 Ni/Mn/Fe-based ternary LTMOs

As the cathode material for SIBs, O3-$NaNi_{1/2}Mn_{1/2}O_2$ exhibited stable circulation performance when the voltage is below 4.0 V.[106] Fe-substitution in O3-$NaNi_{1/2}Mn_{1/2}O_2$ helps to enhance structural stability by forming stable OP2 phase in high voltage region (over 4.0 V). Johnson and co-workers reported O3-type layered $NaNi_{1/3}Fe_{1/3}Mn_{1/3}O_2$ as promising positive electrode candidates with an appreciable capacity of 130 mAh g^{-1} (0.1 C) while full cell based on $NaNi_{1/3}Fe_{1/3}Mn_{1/3}O_2$ cathode with hard carbon anode exhibited 100 mAh g^{-1} reversible capacity at 0.5 C between 2.0-4.0 V for 150 cycles with a smooth voltage profile.[125] Yuan *et al* reported a series of $NaFe_x(Ni_{0.5}Mn_{0.5})_{1-x}O_2$ cathode materials, among which, $NaFe_{0.2}Ni_{0.4}Mn_{0.4}O_2$ showed optimal electrochemical performance and stable cyclability due to the unique OP2 with smaller interslab distance, which prevented the insertion of solvent molecules and electrolyte anions.[126] Therefore, stable cycling of cathode materials can be obtained in high voltage regions.

Based on the research about a series of O3-type $Na[Ni_{0.75-x}Fe_xMn_{0.25}]O_2$ (x=0.4,

0.45, 0.5, and 0.55), increasing Fe content within a proper scale can lead to an improved cycling stability and rate capability due to the reversible redox reaction of Ni^{2+}/Ni^{4+} and Fe^{3+}/Fe^{4+} couples. As a result, $Na[Ni_{0.25}Fe_{0.5}Mn_{0.25}]O_2$ showed improved electrical conductivity compared with other analogues.[127] Similarly, the electrochemical inactive Mn^{4+} helped to keep the lattice structure during Na^+ (de)intercalation.[128,129] Oh and co-workers developed a SIB full cell with carbon-coated Fe_3O_4 anode, $Na[Ni_{0.25}Fe_{0.5}Mn_{0.25}]O_2$ cathode, and $NaClO_4$ in fluoroethylene carbonate and ethyl methanesulfonate electrolyte, which exhibited improved cycling stability (Fig. 10a and b).[128] To optimize the battery performance of O3-$Na[Ni_{0.25}Fe_{0.5}Mn_{0.25}]O_2$ cathode material, Li-substituted $Na[Li_{0.05}(Ni_{0.25}Fe_{0.25}Mn_{0.5})_{0.95}]O_2$ delivered up to a capacity of 180.1 mAh g^{-1} at 0.1 C rate and retained 89.6% capacity at 0.2 C (92.1% 0.5 C) over 40 cycles. The addition of lithium can reduce the Fe^{3+} migration from the transition metal layer to Na layer during charge/discharge cycling.[130] O3-$NaNi_{1/3}Fe_{1/3}Mn_{1/3}O_2$ was also developed as promising air-stable cathode for SIB with a reversible capacity of 120 mAh g^{-1}, when a cut-off voltage was limited below 4.0 V.[131] $NaNi_{1/3}Fe_{1/3}Mn_{1/3}O_2$ went through a continuous phase transition process during charge/discharge cycling due to the 2D Fe/Ni X-ray absorption near edge structure maps in Fig. 10c.

Ca-substitution for partial Na^+ benefited from Na^+ diffusion and improved the cycling stability of $NaNi_{1/3}Fe_{1/3}Mn_{1/3}O_2$ material by enlarging the distance between Na^+ layers. Liao group investigated the Ca-substituted O3-$Na_{1-x}Ca_{x/2}Ni_{1/3}Fe_{1/3}Mn_{1/3}O_2$ (x=0, 0.05, 0.1), which demonstrated an improved cycling stability due to the enlarged alkali layer distance. The O3-$Na_{0.9}Ca_{0.05}Ni_{1/3}Fe_{1/3}Mn_{1/3}O_2$ delivered the optimized reversible capacity of 116.3 mAh g^{-1} at 1 C and capacity retention of 92% after 200 cycles as shown in Fig. 10d and e, while it went through a high reversible O3-P3-P3-O3 phase transition during Na^+ insertion/extraction process.[132]

O3-$Na(Mn_{0.25}Fe_{0.25}Co_{0.25}Ni_{0.25})O_2$ was synthesized with excellent electrochemical performance including an initial discharge capacity of 180 mA h g^{-1} between 1.9V and 4.3 V at C/10 and 578 Wh kg^{-1} specific energy density.[133] Its

Ti-substituted compound O3-$NaNi_{1/4}Co_{1/4}Fe_{1/4}Mn_{1/8}Ti_{1/8}O_2$ demonstrated an improved cycling stability with 91% capacity retention at 4 C after 300 cycles and improved rate performance due to the full utilization of Ni^{2+}/Ni^{3+}, Fe^{3+}/Fe^{4+}, and Co^{3+}/Co^{4+} redox couples during charge/discharge cycles.[134]

As the promising cathode material candidate for SIBs, Ni/Mn-based LTMOs exhibit high specific capacity and rate capability. However, this kind of materials always suffer from irreversible phase transition, leading to structure evolution, volume change, and capacity fading during charge/discharge cycling. Cation substitution is widely applied to improve electrochemical performance and air stability without capacity sacrifice by suppressing the phase transition process. Attentions should also be paid to reduce the cost caused by cation substitution. Other methods including surface coating and compounding are also applied to improve the battery performance.

6. Prospects

In last 5 years, great achievements and progresses have been made in LTMOs cathode materials for application in SIBs. However, from academic investigation to practical application, there remains a long way to go. Lots of works still need to be done to explore the big family of LTMOs. Considerations should be focused on improving the overall electrochemical performance, increasing air stability, reducing cost, and enhancing environmental friendliness.

Considering the structural differences between P2-type and O3-type materials, it is better to investigate them separately. As cathode materials, P2-type LTMOs exhibit good cycling stability and high ion conductivity due to their structural merits. During Na^+ insertion and extraction, P2-type LTMOs usually experience P2-O2 single phase transition, which can be suppressed or transferred to high reversible P2-OP4 process by effective structure design methods. As a result, the P2 layered structure is highly retained, leading to good cycling stability. The P2-type layered structure also provides an open path for the diffusion of Na^+ resulting in low energy barrier of Na^+ migration

and high ionic conductivity. However, P2 type structure always suffers from initial irreversible capacity and undesirable specific capacity due to its sodium deficiency. Comparing to P2-type LTMOs, O3-type cathodes possess the advantages of high energy density, high specific capacity due to its wide operating voltage window and matching well with anode material in full SIB based on its high initial coulombic efficiency. In O3-type LTMOs, Na^+ ions need to overcome large energy barrier when migrating from one octahedral site to another through edge-sharing tetrahedral site between them. Accordingly, O3-type LTMOs exhibit low ion conductivity.

Besides overall electrochemical performance, air stability is another unavoidable factor to influence the development of LTMOs. Because of the large distance between sodium layers, this kind of materials usually intake H_2O/CO_2 from air, followed by undesired chemical reaction. As a result, the electrochemical performance of cathode degrades due to the formation of inactive $NaOH/Na_2CO_3$. From the view of cost control and environment friendliness, using raw materials containing cost effective and non-toxic elements such as Fe and Mn, instead of expensive and poisonous element like Co, is more important for the sustainable development of LTMOs. Improving energy density of this kind of cathode material is another effective method to reduce cost.

Overall electrochemical performance, no doubly, is an important property of SIBs, while production cost is an essential factor as well. Balancing the relationship between them is both the remaining challenge and a key link of the commercialization of SIBs. Most of recent works in this area, however, only focused performance improvements instead of cost reduction. In Ni/Mn co-based LTMOs materials, the most direct method for reducing cost is to enlarge the relative ratio of Mn as well as cutting down the use of expensive materials like Co, Ni, and Ti et al on the premise of maintaining performance in cation substitution design routes. Accordingly, natural carbonaceous materials need to be developed to composite with LTMOs instead of expensive graphene or carbon nanotube materials. By doing this, the cost of SIBs would be sharply reduced, followed by the contribution to the environment. Besides,

another effective method for reducing cost is process-simplifying. Once the fabrication of material preparation and the package of cells is simple enough, the cost of product line and time would be sharply reduced.

In the future, efforts should be made in both innovating structure design approaches and investigating structure revolution mechanism during cycling to meet these requirements. For structure design, besides the most popular and effective cation substitution, other methods such as micro/nano-composites with other systems and surface coating protect layers, should be strongly attempted to reduce the irreversible structure change and improve the electrochemical performance during charge/discharge cycling. For P2-type LTMOs, attention should be paid to improve initial coulombic efficiency while for O3-type LTMOs, it is more important to control the complex phase transition process and enhance cycling stability by reasonable structure design method. For example, new type of $K_{0.7}Fe_{0.5}Mn_{0.5}O_2$ have been developed as one cathode material for SIBs.[135] Zhou and co-workers developed stable P3-type stacking to deliver excellent cycling performance by the cation-mixing nature.[136] Structure design approaches should be also developed focusing on reducing the interlayer distance to suppress the reaction between LTMOs and ambient air. For reaction mechanism, intensive studies of the relationship between battery performance and structure revolution should be made to accelerate the commercialization of SIBs fundamentally. Advanced *in situ* measurement techniques such as in situ TEM should be applied to further explore the real reaction mechanism and the evolution of crystal structure during charge/discharge cycling to solve the existed issues like irreversible capacity loss during initial cycles. At present, the battery properties of cathode materials by half-cell test in most of the recent work are quite different from the practical full cells. Therefore, attentions should be paid to strengthen the combination test between cathode materials and other parts of SIBs including anode materials, electrolyte additives, binders *etc.*

7. Conclusion

SIBs have extensive application potential in both mobile and stationary EES systems due to their elemental abundance, cost effectiveness and same working mechanism with LIBs. LTMOs are promising cathode materials for SIBs thanks to high battery performance. But large ionic radius of Na^+ always leads to complex structural transformation of cathode materials during Na^+ insertion/extraction process, resulting in capacity fading, stability decreasing, and volume change *etc*. To maintain excellent battery performance and increasing cycle life, cation substitution has been used to enhance the structure stability of LTMOs by suppressing phase transitions during Na^+ intercalation/deintercalation. At present, Ni/Mn-based materials show improved cell performance compared to other kinds of materials because the full use of $Ni^{2+}/Ni^{3+}/Ni^{4+}$ redox reaction can provide relative high working voltage and high specific capacity, and inactive Mn^{4+} maintains the crystal structure resulting in retention of reversible capacity and long cycling life. Among the reported LTMOs for SIBs, O3-$NaNi_{0.5}Mn_{0.2}Ti_{0.3}O_2$ and O3-$NaNi_{1/3}Fe_{1/3}Mn_{1/3}O_2$ demonstrated the most improved electrochemical performance including large reversible specific capacity, cycling stability, high rate performance, and air-stable properties as well as large-scale production perspectives including cost effective and green raw materials, facile synthesis methods. Although SIBs own the advantages of low-cost and long lifetime, unsatisfied cell performance still hinders the practical commercialization of this EES system. The rapid growth in recent years indicate the bright future of LTMOs as cathode materials for SIBs.

Acknowledgements

This work was supported by National Natural Science Foundation of China (NSFC) (11574113, 11374123, 11104106); Science and Technology Planning Project of Jilin Province (20180101238JC, 20170204076GX, 20180101006JC, 20190103041JH), Post-Doctoral Innovative Talent Support Program (BX20180127). Q.Z. acknowledges financial support from AcRF Tier 1 (RG 111/17, RG 2/17, RG 114/16, RG 8/16) and

Tier 2 (MOE 2017-T2-1-021 and MOE 2018-T2-1-070), Singapore.

References

1 (a) M. Armand and J. M. Tarascon, *Nature*, 2008, **451**, 652-657; (b) Y. -K. Sun, Z. Chen, H. -J. Noh, D. -J. Lee, H. -G. Jung, Y. Ren, S. Wang, C. S. Yoon, S. -T. Myung and K. Amine, *Nat. Mater.*, 2012, **11**, 942-947。

2 P. -F. Wang, Y. You, Y. -X. Yin, and Y. -G. Guo, *Adv. Energy Mater.*, 2018, **8**, 1701912.

3 D. Kim, M. Cho. and K. Cho, *J. Mater. Chem. A*, 2018, **6**, 18036-18043.

4 (a) J. Xie and Q. Zhang, *Small*, 2019, DOI: 10.1002/smll.201805061; (b) Z. Wu, J. Xie, Z. J. Xu, S. Zhang and Q. Zhang, *J. Mater. Chem. A*, 2019, **7**, 4259 – 4290; (c) J. Xie, Z. Wang, Z. J. Xu and Q. Zhang, *Adv. Energy Mater.* 2018, **8**, 1703509; (d) J. Xie and Q. Zhang, *J. Mater. Chem. A*, 2016, **4**, 7091-7106; (e) Z.-Q. Lin, J. Xie, B. Zhang, J. Li, J.-N. Weng, R.-B. Song, X. Huang, H. Zhang, H. Li, Y. Liu, Z. J. Xu, W. Huang and Q. Zhang, *Nano Energy*, 2017, **41**, 117-127; (f) J. Xie, P. Gu and Q. Zhang, *ACS Energy Lett.*, 2017, **2**, 1985–1996; (g) J. Xie, C.-E Zhao, Z. Lin, P.-Y. Gu and Q. Zhang, *Chem. Asian J.* 2016, **11**, 1489-1511; (h) X. Zhan, Z. Chen and Q. Zhang, *J. Mater. Chem. A*, 2017, **5**, 14463 – 14479.

5 W. Ko, T. Park, H. Park, Y. Lee, K. E. Leeb and J. Kim, *J. Mater. Chem. A*, 2018, **6**, 17095-17100.

6 V. Palomares, P. Serras, I. Villaluenga, K.B. Hueso, J. Carretero-González, and T. Rojo, *Energy & Environ. Sci*., 2012, **5**, 5884-5901.

7 C. Nithy and S. Gopukumar, *Wiley Interdisciplinary Reviews: Energy and Environment*, 2014, **4**, 253-278.

8 P. Hou, H. Zhang, Z. Zi, L. Zhang and X. Xu, *J. Mater. Chem. A*, 2017, **5**, 4254-4279.

9 D. Kundu, E. Talaie, V. Duffort, and L. F. Nazar, *Angew Chem. Int. Edit.*, 2015, **54**, 3431-3448.

10 J. H. Lee, C. S. Yoon, J. -Y. Hwang, S. -J. Kim, F. Maglia, P. Lamp, S. -T. Myung and Y. -K. Sun, *Energy & Environ. Sci.*, 2016, **9**, 2152-2158.

11 J. B. Goodenough and Y. Kim, *Chem. Mater.*, 2010, **22**, 587-603.

12 V. Etacheri, R. Marom, R. Elazari, G. Salitra and D. Aurbach, *Energy & Environ. Sci.*, 2011, **4**, 3243-3262.

13 Y. Xiao, S. H. Lee, and Y. -K. Sun, *Adv. Energy Mater.*, 2017, **7**, 1601329.

14 S. -W. Kim, D. -H. Seo, X. Ma, G. Ceder and K. Kang, *Adv. Energy Mater.*, 2012, **2**, 710-721.

15 N. Yabuuchi, K. Kubota, M. Dahbi and S. Komaba, *Chem. Rev.*, 2014, **114**, 11636-11682.

16 H. Kim, H. Kim, Z. Ding, M. H. Lee, K. Lim, G. Yoon and K. Kang, *Adv. Energy Mater.*, 2016, **6**, 1600943.

17 M. Lao, Y. Zhang, W. Luo, Q. Yan, W. Sun and S. X. Dou, *Adv. Mater.*, 2017, **29**, 1700622.

18 M. Okoshi, Y. Yamada, A. Yamada and H. Nakai, *J. Electrochem. Soc.*, 2013, **160**, A2160-A2165.

19 Y. You and A. Manthiram, *Adv. Energy Mater.*, 2018, **8**, 1701785.

20 Y. Xiao, P. -F. Wang, Y. -X. Yin, Y.-F. Zhu. X. Yang, X.- D. Zhang, Y. Wang, X. -D. Guo, B. -H. Zhong and Y. -G. Guo, *Adv. Energy Mater.*, 2018, **8**, 1800492.

21 D. Kundu, E. Talaie, V. Duffort and L. F. Nazar, *Angew. Chem.*, 2015, **127**, 3495-3513.

22 S. Guo, J. Yi, Y. Sun and H. Zhou, *Energy & Environ. Sci.*, 2016, **9**, 2978-3006.

23 J.-S. Park, J. Kim, J. H. Jo and S.-T. Myung. *J. Mater. Chem. A*, 2018, **6**, 16627 – 16637.

24 Y. Xiao, P. -F. Wang, Y. -X. Yin, Y.-F. Zhu. Y. -B. Niu, X.- D. Zhang, J. Zhang, X. Yu, X. -D. Guo, B. -H. Zhong and Y. -G. Guo, *Adv. Mater.* 2018, **30**, 1803765.

25 J. Liu , K. Tang , K. P. Song, P. A. van Aken, Y. Yu , J. Maier, *Nanoscale*, 2014, **6**, 5081.

26 C. Li, X. Miao, W. Chu, P. Wua, D. G. Tong, *J. Mater. Chem. A* 2015, **3**, 8265..

27 T. Boyadzhieva, V. Koleva, E. Zhecheva, D. Nihtianova, L. Mihaylov, R. Stoyanova, *RSC Adv*. 2015, **5**, 87694.

28 P. Singh, K. Shiva, H. Celio, J. B. Goodenough, *Energy Environ. Sci.* 2015, **8**, 3000..

29 H. Kim, R. A. Shakoor, C. Park, S. Y. Lim, J.-S. Kim, Y. N. Jo, W. Cho, K. Miyasaka, R. Kahraman, Y. Jung, J. W. Choi, *Adv. Funct. Mater.* 2013, **23**, 1147.

30 M. Ling, F. Li, H. Yi, X. Li, G. Hou, Q. Zheng and H. Zhang, *J. Mater. Chem. A*, 2018, **6**, 24201-24209.

31 T..Matsuda, M. Takachi , Y. Moritomo , *Chem. Commun.* 2013, **49**, 2750.

32 L. Wang, Y. Lu, J. Liu, M. Xu, J. Cheng, D. Zhang, J. B. Goodenough, *Angew. Chem. Int. Ed*. 2013, **52**, 1964.

33 X. Y. Wu, W. W. Deng, J. F. Qian, Y. L. Cao, X. P. Ai, H. X. Yang, *J. Mater. Chem. A* 2013, 1, 10130.

34 H. Ye, C.-Y. Wang, T.-T. Zuo, P.-F. Wang, Y.-X. Yin, Z.-J. Zheng, P. Wang, J. Cheng, F.-F. Cao and Y.-G. Guo, Nano Energy 48 (2018) 369-376.

35 A. Mendiboure, C. Delmas and P. Hagenmuller, *J. Solid State Chem.*, 1985, **57**, 323-331.

36 S. Kumakura, Y. Tahara, K. Kubota, K. Chihara and S. Komaba, *Angew Chem. Int. Edit.*, 2016, **55**, 12760-12763.

37 A. Caballero, L. Hernán, J. Morales, L. Sánchez, J. Santos Peña and M. A. G. Aranda, *J. Mater. Chem.*, 2002, **12**, 1142-1147.

38 M. H. Han, E. Gonzalo, M. Casas-Cabanas and T. Rojo, *J. Power Sources*, 2014, **258**, 266-271.

39 Z. Lu and J. R. Dahn, *J. Electrochem. Soc.*, 2001, **148**, A1225-A1229.

40 D. H. Lee, J. Xu and Y. S. Meng, *Phys. Chem. Chem. Phys.*, 2013, **15**, 3304-3312.

41 E. Gonzalo, M. H. Han, J. M. López del Amo, B. Acebedo, M. Casas-Cabanas and T. Rojo, *J. Mater. Chem. A*, 2014, **2**, 18523-18530.

42 J. S. Thorne, R. A. Dunlap and M. N. Obrovac, *J. Electrochem. Soc.*, 2013, **160**, A361-A367.

43 B. Mortemard de Boisse, D. Carlier, M. Guignard and C. Delmas, *J. Electrochem. Soc.*, 2013, **160**, A569-A574.

44 N. Yabuuchi, M. Kajiyama, J. Iwatate, H. Nishikawa, S. Hitomi, R. Okuyama, R. Usui and Y. Yamada, S. Komaba, *Nat. Mater.*, 2012, **11**, 512-517.

45 X. Ma, H. Chen and G. Ceder, *J. Electrochem. Soc.*, 2011, **158**, A1307-A1312.

46 L. Baggetto, K. J. Carroll, R. R. Unocic, C. A. Bridges, Y. S. Meng and G. M. Veith, *ECS Transactions*, 2014, **58**, 47-57.

47 T. Ma, G. -L. Xu, X. Zeng, Y. Li, Y. Ren, C. Sun, S. M. Heald, J. Jorne, K. Amine and Z. Chen, *J. Power Sources*, 2017, **341**, 114-121.

48 J. -Y. Li, H. -Y. Lü, X. -H. Zhang, Y. -M. Xing, G. Wang, H. -Y. Guan and X. -L. Wu, *Chem. Eng. J.*, 2017, **316**, 499-505.

49 E. de la Llave, E. Talaie, E. Levi, P. K. Nayak, M. Dixit, P. T. Rao, P. Hartmann, F. Chesneau, D. T. Major, M. Greenstein, D. Aurbach and L. F. Nazar, *Chem. Mater. Chem. Mater.*, 2016, **28**, 9064-9076.

50 N. Yabuuchi, R. Hara, M. Kajiyama, K. Kubota, T. Ishigaki, A. Hoshikawa and S. Komaba, *Adv. Energy Mater.*, 2014, **4**, 1301453.

51 J. Billaud, G. Singh, A. R. Armstrong, E. Gonzalo, V. Roddatis, M. Armand, T. Rojo and P. G. Bruce, *Energy & Environ. Sci.*, 2014, **7**, 1387-1391.

52 D. Buchholz, C. Vaalma, L. G. Chagas and S. Passerini, *J. Power Sources*, 2015, **282**, 581-585.

53 N. Sharma, N. Tapia-Ruiz, G. Singh, A. R. Armstrong, J. C. Pramudita, H. E. A. Brand, J. Billaud, P. G. Bruce and T. Rojo, *Chem. Mater.*, 2015, **27**, 6976-6986.

54 R. J. Clément, J. Billaud, A. Robert Armstrong, G. Singh, T. Rojo, P. G. Bruce and C. P. Grey, *Energy & Environ. Sci.*, 2016, **9**, 3240-3251.

55 W. Kang, Z. Zhang, P. -K. Lee, T. -W. Ng, W. Li, Y. Tang, W. Zhang, C. -S. Lee and D. Y. W. Yu, *J. Mater. Chem. A*, 2015, **3**, 22846-22852.

56 W. -L. Pang, X. -H. Zhang, J. -Z. Guo, J. -Y. Li, X. Yan, B. -H. Hou, H. -Y. Guan and X. -L. Wu, *J. Power Sources*, 2017, **356**, 80-88.

57 Z. -Y. Li, R. Gao, J. Zhang, X. Zhang, Z. Hu and X. Liu, *J. Mater. Chem. A*, 2016, **4**, 3453-3461.

58 N. Yabuuchi, R. Hara, K. Kubota, J. Paulsen, S. Kumakura and S. Komaba, *J. Mater. Chem. A*, 2014, **2**, 16851-16855.

59 Y. Zhong, X. Xia, J. Zhan, X. Wang and J. Tu, *J. Mater. Chem. A*, 2016, **4**, 11207-11213.

60 I. Hasa, D. Buchholz, S. Passerini and J. Hassoun, *ACS Appl. Mater. Inter.*, 2015, **7**, 5206-5212.

61 B. M. de Boisse, D. Carlier, M. Guignard and C. Delmas, *J. Electrochem. Soc.*, 2013, **160**, A569-A574.

62 G. Singh, J. M. López del Amo, M. Galceran, S. Pérez-Villar and T. Rojo, *J. Mater. Chem. A*, 2015, **3**, 6954-6961.

63 J. Martinez De Ilarduya, L. Otaegui, J. M. López del Amo, M. Armand and G. Singh, *J. Power Sources*, 2017, **337**, 197-203.

64 M. H. Han, E. Gonzalo, N. Sharma, J. M. López del Amo, M. Armand, M. Avdeev, J. J. Saiz Garitaonandia and T. Rojo, *Chem. Mater.*, 2016, **28**, 106-116.

65 Y. Li, Z. Yang, S. Xu, L. Mu, L. Gu, Y. S. Hu, H. Li and L. Chen, *Adv. Sci.*, 2015, **2**, 1500031.

66 L. Mu, S. Xu, Y. Li, Y. S. Hu, H. Li, L. Chen and X. Huang, *Adv. Mater.*, 2015, **27**, 6928-6933.

67 M. Bianchini, E. Gonzalo, N. E. Drewett, N. Ortiz-Vitoriano, J. M. López del Amo, F. J. Bonilla, B. Acebedo and T. Rojo, *J. Mater. Chem. A*, 2018, **6**, 3552-3559.

68 J. M. Paulsen and J. R. Dahn, *Solid State Ionics*, 1999, **126**, 3-24.

69 X. Wang, M. Tamaru, M. Okubo and A. Yamada, *J. Phys. Chem. C*, 2013, **117**, 15545-15551.

70 N. Bucher, S. Hartung, J. B. Franklin, A. M. Wise, L. Y. Lim, H. -Y. Chen, J. N. Weker, M. F. Toney and M. Srinivasan, *Chem. Mater.*, 2016, **28**, 2041-2051.

71 Y. -T. Zhou, X. Sun, B. -K. Zou, J. -Y. Liao, Z. -Y. Wen and C. -H. Chen, *Electrochim. Acta*, 2016, **213**, 496-503.

72 P. Yang, C. Zhang, M. Li, X. Yang, C. Wang, X. Bie, Y. Wei, G. Chen and F. Du, *J. Mater. Chem. A*, 2015, **16**, 3408-3412.

73 Y. -E. Zhu, X. Qi, X. Chen, X. Zhou, X. Zhang, J. Wei, Y. Hu and Z. Zhou, *J. Mater. Chem. A*, 2016, **4**, 11103-11109.

74 D. Carlier, J. H. Cheng, R. Berthelot, M. Guignard, M. Yoncheva, R. Stoyanova, B. J. Hwang and C. Delmas, *Dalton T.*, 2011, **40**, 9306-9312.

75 Y. Shen, S. Birgisson and B. B. Iversen, *J. Mater. Chem. A*, 2016, **4**, 12281-12288.

76 Y. H. Jung, A. S. Christiansen, R. E. Johnsen, P. Norby and D. K. Kim, *Adv. Funct. Mater.*, 2015, **25**, 3227-3237.

77 L. Liu, X. Li, S. -H. Bo, Y. Wang, H. Chen, N. Twu, D. Wu and G. Ceder, *Adv. Energy Mater.*, 2015, 5 1500944.

78 J. S. Thorne, R. A. Dunlap and M. N. Obrovac, *J. Electrochem. Soc.*, 2014, **161**, A2232-A2236.

79 L. Wang, J. Wang, X. Zhang, Y. Ren, P. Zuo and G. Yin, J. Wang, *Nano Energy*, 2017, **34**, 215-223.

80 D. Yuan, X. Liang, L. Wu, Y. Cao, X. Ai, J. Feng and H. Yang, *Adv. Mater.*, 2014, **26**, 6301-6306.

81 J. Ma, S. -H. Bo, L. Wu, Y. Zhu, C. P. Grey and P. G. Khalifah, *Chem. Mater.*, 2015, **27**, 2387-2399.

82 D. S. Bhange, G. Ali, D. -H. Kim, D. A. Anang, T. J. Shin, M. -G. Kim, Y. -M. Kang, K. Y. Chung and K. -W. Nam, *J. Mater. Chem. A*, 2017, **5**, 1300-1310.

83 H. Yu, S. Guo, Y. Zhu, M. Ishida and H. Zhou, *Chem. Commun.*, 2014, **50**, 457-459.

84 H. Wang, Y. Xiao, C. Sun, C. Lai and X. Ai, *RSC Adv.*, 2015, **5**, 106519-106522.

85 Y. Nanba, T. Iwao, B. M. d. Boisse, W. Zhao, E. Hosono, D. Asakura, H. Niwa, H. Kiuchi, J. Miyawaki, Y. Harada, M. Okubo and A. Yamada, *Chem. Mater.*, 2016, **28**, 1058-1065.

86 S. Guo, H. Yu, P. Liu, Y. Ren, T. Zhang, M. Chen, M. Ishida and H. Zhou, *Energy & Environ. Sci.*, 2015, **8**, 1237-1244.

87 X. Wang, G. Liu, T. Iwao, M. Okubo and A. Yamada, *J. Phys. Chem. C*, 2014, **118**, 2970-2976.

88 P. Vassilaras, D. -H. Kwon, S. T. Dacek, T. Shi, D. -H. Seo, G. Ceder and J. C. Kim, *J. Mater. Chem. A*, 2017, **5**, 4596-4606.

89 P. Vassilaras, A. J. Toumar and G. Ceder, *Electrochem. Commun.*, 2014, **38**, 79-81.

90 G. Singh, F. Aguesse, L. Otaegui, E. Goikolea, E. Gonzalo, J. Segalini and T. Rojo, *J. Power Sources*, 2015, **273**, 333-339.

91 J. Wang, X. He, D. Zhou, F. Schappacher, X. Zhang, H. Liu, M. C. Stan, X. Cao, R. Kloepsch, M. S. Sofy, G. Schumacher and J. Li, *J. Mater. Chem. A*, 2016, **4**, 3431-3437.

92 J. -L. Yue, Y. -N. Zhou, X. Yu, S. -M. Bak, X. -Q. Yang and Z. -W. Fu, *J. Mater. Chem. A*, 2015, **3**, 23261-23267.

93 C. Ma, J. Alvarado, J. Xu, R. J. Clement, M. Kodur, W. Tong, C. P. Grey and Y. S. Meng, *J. Am. Chem. Soc.*, 2017, **139**, 4835-4845.

94 P. -F. Wang, Y. You, Y. -X. Yin, Y. -S. Wang, L. -J. Wan, L. Gu and Y. -G. Guo, *Angew. Chem., Int. Ed.*, 2016, **55**, 7445-7449.

95 R. J. Clément, J. Xu, D. S. Middlemiss, J. Alvarado, C. Ma, Y. S. Meng and C. P. Grey, *J. Mater. Chem. A*, 2017, **5**, 4129-4143.

96 J. Xu, D. H. Lee, R. J. Clément, X. Yu, M. Leskes, A. J. Pell, G. Pintacuda, X. -Q. Yang, C. P. Grey and Y. S. Meng, *Chem. Mater.*, 2014, **26**, 1260-1269.

97 L. Wang, Y. -G. Sun, L. -L. Hu, J. -Y. Piao, J. Guo, A. Manthiram, J. Ma and A. -M. Cao, *J. Mater. Chem. A*, 2017, **5**, 8752-8761.

98 L. Zheng, J. Li and M. N. Obrovac, *Chem. Mater.*, 2017, **29**, 1623-1631.

99 X. Wu, J. Guo, D. Wang, G. Zhong, M. J. McDonald and Y. Yang, *J. Power Sources*, 2015, **281**, 18-26.

100 X. -H. Zhang, W. -L. Pang, F. Wan, J. -Z. Guo, H. -Y. Lü, J. -Y. Li, Y. -M. Xing, J. -P. Zhang and X. -L. Wu, *ACS Appl. Mater. Inter.*, 2016, **8**, 20650-20659.

101 H. Yoshida, N. Yabuuchi, K. Kubota, I. Ikeuchi, A. Garsuch, M. Schulz-Dobrick and S. Komaba, *Chem. Commun.*, 2014, **50**, 3677-3680.

102 Y. Liu, X. Fang, A. Zhang, C. Shen, Q. Liu, H. A. Enaya and C. Zhou, *Nano Energy*, 2016, **27**, 27-34.

103 J. Alvarado, C. Ma, S. Wang, K. Nguyen, M. Kodur and Y. S. Meng, *ACS Appl. Mater. Inter.*, 2017, **9**, 26518-26530.

104 J. H. Jo, J. U. Choi, A. Konarov, H. Yashiro, S. Yuan, L. Shi, Y. -K. Sun and S. -T. Myung, *Adv. Funct. Mater.*, 2018, **28**, 1705968.

105 S. Komaba, N. Yabuuchi, T. Nakayama, A. Ogata, T. Ishikawa and I. Nakai, *Inorg. Chem.*, 2012, **51**, 6211-6220.

106 R. Fielden and M. N. Obrovac, *J. Electrochem. Soc.*, 2015, **162**, A453-A459.

107 J. Cabana, N. A. Chernova, J. Xiao, M. Roppolo, K. A. Aldi, M. S. Whittingham and C. P. Grey, *Inorg. Chem.*, 2013, **52**, 8540-8550.

108 P. F. Wang, H. R. Yao, X. Y. Liu, J. N. Zhang, L. Gu, X. Q. Yu, Y. X. Yin and Y. G. Guo, *Adv. Mater.*, 2017, **29**, 1700210.

109 H. R. Yao, P. F. Wang, Y. Gong, J. Zhang, X. Yu, L. Gu, C. OuYang, Y. X. Yin, E. Hu, X. Q. Yang, E. Stavitski, Y. G. Guo and L. J. Wan, *J. Am. Chem. Soc.*, 2017, **139**, 8440-8443.

110 J. Deng, W. -B. Luo, X. Lu, Q. Yao, Z. Wang, H. -K. Liu, H. Zhou and S. -X. Dou, *Adv. Energy Mater.*, 2018, **8**, 1701610.

111 E. Lee, J. Lu, Y. Ren, X. Luo, X. Zhang, J. Wen, D. Miller, A. De Wahl, S. Hackney, B. Key, D. Kim, M. D. Slater and C. S. Johnson, *Adv. Energy Mater.*, 2014, **4**, 1400458.

112 Z. -Y. Li, J. Zhang, R. Gao, H. Zhang, Z. Hu and X. Liu, *ACS Appl. Mater. Inter.*, 2016, **8**, 15439-15448.

113 L. G. Chagas, D. Buchholz, C. Vaalma, L. Wu and S. Passerini, *J. Mater. Chem. A*, 2014, **2**, 20263-20270.

114 S. Doubaji, M. Valvo, I. Saadoune, M. Dahbi and K. Edström, *J. Power Sources*, 2014, **266**, 275-281.

115 X. Sun, X. -Y. Ji, H. -Y. Xu, C. -Y. Zhang, Y. Shao, Y. Zang and C. -H. Chen, *Electrochim. Acta.*, 2016, **208**, 142-147.

116 R. Kataoka, T. Mukai, A. Yoshizawa, K. Inoue, T. Kiyobayashi and T. Sakai, *J. Electrochem. Soc.*, 2015, **162**, A553-A558.

117 J. Yoshida, E. Guerin, M. Arnault, C. Constantin, B. Mortemard de Boisse, D. Carlier, M. Guignard and C. Delmas, *J. Electrochem. Soc.*, 2014, **161**, A1987-A1991.

118 J. -Y. Hwang, C. S. Yoon, I. Belharouak and Y. -K. Sun, *J. Mater. Chem. A*, 2016, **4**, 17952-17959.

119 H. Xu, J. Zong, S. Chen, F. Ding, Z. -W. Lu and X. -J. Liu, *Ceram. Int.*, 2016, **42**, 12521-12524.

120 M. Sathiya, K. Hemalatha, K. Ramesha, J. M. Tarascon and A. S. Prakash, *Chem. Mater.*, 2012, **24**, 1846-1853.

121 D. Yuan, W. He, F. Pei, F. Wu, Y. Wu, J. Qian, Y. Cao, X. Ai, H. Yang and *J. Mater. Chem. A*, 2013, **1**, 3895-3899.

122 Z. -Y. Li, R. Gao, L. Sun, Z. Hu, X. Liu and *J. Mater. Chem. A*, 2015, **3**, 16272-16278.

123 K. Kaliyappan, J. Liu, A. Lushington, R. Li and X. Sun, *ChemSusChem*, 2015, **8**, 2537-2543.

124 Rangasamy, L. Zhang, J. W. Seo, J. -P. Locquet and S. Thayumanasundaram, *Electrochim. Acta.*, 2017, **237**, 29-36.

125 D. Kim, E. Lee, M. Slater, W. Lu, S. Rood and C. S. Johnson, *Electrochem. Commun.*, 2012, **18**, 66-69.

126 D. D. Yuan, Y. X. Wang, Y. L. Cao, X. P. Ai and H. X. Yang, *ACS Appl. Mater. Inter.*, 2015, **7**, 8585-8591.

127 J. -Y. Hwang, S. -T. Myung, D. Aurbach and Y. -K. Sun, *J. Power Sources*, 2016, **324**, 106-112.

128 S. M. Oh, S. T. Myung, C. S. Yoon, J. Lu, J. Hassoun, B. Scrosati, K. Amine and Y. K. Sun, *Nano Lett.*, 2014, **14**, 1620-1626.

129 I. Hasa, D. Buchholz, S. Passerini, B. Scrosati and J. Hassoun, *Adv. Energy Mater.*, 2014, **4**, 1400083.

130 S. -M. Oh, S. -T. Myung, J. -Y. Hwang, B. Scrosati, K. Amine and Y. -K. Sun, *Chem. Mater.*, 2014, **26**, 6165-6171.

131 Y. Xie, H. Wang, G. Xu, J. Wang, H. Sheng, Z. Chen, Y. Ren, C. -J. Sun, J. Wen, J. Wang, D. J. Miller, J. Lu, K. Amine and Z. -F. Ma, *Adv. Energy Mater.*, 2016, **6**, 1601306.

132 L. Sun, Y. Xie, X. Z. Liao, H. Wang, G. Tan, Z. Chen, Y. Ren, J. Gim, W. Tang, Y. S. He, K. Amine and Z. F. Ma, *Small*, 2018, **14**, 1704523.

133 X. Li, D. Wu, Y. -N. Zhou, L. Liu, X. -Q. Yang and G. Ceder, *Electrochem. Commun.*, 2014, **49**, 51-54.

134 J. -L. Yue, W. -W. Yin, M. -H. Cao, S. Zulipiya, Y. -N. Zhou and Z. -W. Fu, *Chem. Commun*., 2015, **51**, 15712-15715.

135 X. Wang, P. Hu, C. Niu, J. Meng, X. Xu, X. Wei, C. Tang, W. Luo, L. Zhou, Q. An and L. Mai, *Nano Energy*, 2017, **35**, 71-78.

136 S. Guo, Y. Sun, P. Liu, J. Yi, P. He, X. Zhang, Y. Zhu, R. Senga, K. Suenaga, M. Chen and H. Zhou, *Sci. Bulletin*, 2018, **63**, 376-384.

Table 1 Summery of the battery performance of recent reported LTMOs cathode materials for SIBs

Material	Voltage window(V)	Practical capacity [mA h g^{-1}]	Phase transition	Capacity retention	Year
P2-$Na_{2/3}Fe_{2/3}Mn_{1/3}O_2$[41]	1.5–4.2	151 (25 mA/ g)	P2–OP4	81.3% (10 cycles)	2014
P2-$Na_{2/3}Fe_{1/2}Mn_{1/2}O_2$[44]	1.5–4.2	190 (12 mA/g)	P2–OP4	79% (30 cycles)	2012
O3-$NaFe_{1/2}Mn_{1/2}O_2$[44]	1.5–4.2	110 (12 mA/g)	O3–P3–OP2	60% (30 cycles)	2012
P2-$Na_{0.6}Mn_{0.8}Li_{0.2}O_2$[49]	2.0–4.6	190 (C/15)	P2–O2	100% (100 cycles)	2016
P2-$Na_{0.67}Mn_{0.8}Mg_{0.2}O_2$[51]	1.5–4.0	150 (12 mA/g)	P2–OP4	100% (25 cycles)	2014
P2-$Na_{2/3}Mn_{0.95}Mg_{0.05}O_2$[54]	1.5-4.0	170 (100 mA/g)	P2–OP4-P2′	80% (100 cycles)	2016
P2-$Na_{0.7}MnO_{2.05}$/carbon[59]	1.8-4.4	158.2 (100 mA/g)	P2-O3	88% (100 cycles)	2016
P2-$Na_{7/9}Cu_{2/9}Fe_{1/9}Mn_{2/3}O_2$[65]	2.5–4.2	89 (10 mA/g)	P2	87% (150 cycles)	2015
O3-$Na_{0.90}[Cu_{0.22}Fe_{0.30}Mn_{0.48}]O_2$[66]	2.5–4.05	100 (10 mA/g)	O3–P3–O′3	97% (100 cycles)	2015
P2-$Na_{0.67}Co_{0.5}Mn_{0.5}O_2$[73]	1.5–4.3	147 (17 mA/g)	P2	100% (100 cycles)	2016
P2-$Na_xCo_{0.7}Mn_{0.3}O_2$ (x≈1.0)[75]	4.1-2.0	95 (1 C)	P2-O2	84% (225 cycles)	2016
P2-$Na_{0.7}Fe_{0.4}Mn_{0.4}Co_{0.2}O_2$[76]	1.5–4.5	190 (10 mA/g)	P2–O2	61% (60 cycles)	2015
P2-$Na_{2/3}(Mn_{1/2}Fe_{1/4}Co_{1/4})O_2$ [77]	1.5–4.2	150 (2580 mA/g)	P2-Z-P2	100% (30 cycles)	2015
O'3-$Na_3Ni_2SbO_6$[80]	2.0–4.0	117 (20 mA/g)	O′3–P′3–O1	95% (50 cycles)	2014
O′3-$Na_3Ni_2BiO_6$[82]	2.0–4.0	106 (0.05 C)	O′3–P′3–O1	91% (50 cycles)	2017
O3-$Na_{0.8}Ni_{0.4}Ti_{0.6}O_2$[86]	0.6–3.8	53 (100 mA/g)	O3-P3	75% (150 cycles)	2015
O3-$NaNi_{0.5}Fe_{0.5}O_2$[88]	2.0–3.9	129 (23.5 mA/g)	O3–P3	94% (20 cycles)	2017
O3-$NaFe_{1/3}Ni_{1/3}Ti_{1/3}O_2$[91]	1.5–4.0	117 (10 mA/g)	O3–P3	57% (1000 cycles)	2016
O3-$NaNi_{1/4}Co_{1/4}Fe_{1/4}Ti_{1/4}O_2$[92]	2.0–3.9	116 (12 mA/g)	O3–P3	75% (400 cycles)	2015
P2-$Na_{0.78}Ni_{0.23}Mn_{0.69}O_2$[93]	2.0-4.5	138 (12.1 mA/g)	P2-O2	86.9% (20 cycles)	2017
P2-$Na_{0.67}Mn_{0.67}Ni_{0.28}Mg_{0.05}O_2$[94]	2.5-4.35	123 (17.3 mA/g)	P2	85% (50 cycles)	2016
Al_2O_3 coated P2-$Na_{2/3}[Ni_{1/3}Mn_{2/3}]O_2$[102]	2.5-4.3	160 (86.5 mA/g)	P2-O2	73.2% (300 cycles)	2016
$NaPO_3$-coated $Na_{2/3}[Ni_{1/3}Mn_{2/3}]O_2$[104]	1.5–4.3	194 (20 mA/g)	P2-O2	73% (300 cycles)	2018
O3-$NaNi_{0.5}Mn_{0.2}Ti_{0.3}O_2$[108]	2.0–4.0	135 (12 mA/g)	O3–P3	85% (200 cycles)	2017
O3-$NaNi_{0.45}Cu_{0.05}Mn_{0.4}Ti_{0.1}O_2$[109]	2.0–4.0	124 (24 mA/g)	O3–P3	70.2% (500 cycles)	2017

O3-Na[$Li_{0.05}Mn_{0.50}Ni_{0.30}Cu_{0.10}Mg_{0.05}$]$O_2$ [110]	2.0-4.0	172 (0.1 C)	O3-P3	87.7% (200 cycles)	2018
P2/O3 $Na_{0.7}Li_{0.3}Ni_{0.5}Mn_{0.5}O_{2+d}$ [111]	2.0–4.05	125 (15 mA/g)	P2/O3–P2/O′3–P2/P3–P2/O″3	95% (20 cycles)	2014
O3-$NaNi_{0.25}Fe_{0.5}Mn_{0.25}O_2$ [128]	2.1–3.9	140 (13 mA/g)	O3-P3	90.4% (50 cycles)	2014
P2-$Na_{0.5}$[$Ni_{0.23}Fe_{0.13}Mn_{0.63}$]$O_2$ [129]	1.5-4.6	200 (15 mA/g)	P2-O2	75% (70 cycles)	2014
O3-$Na_{0.9}Ca_{0.05}Ni_{1/3}Fe_{1/3}Mn_{1/3}O_2$ [132]	2.0-4.0	116.3(130 mA/g)	O3-P3	92% (200 cycles)	2018

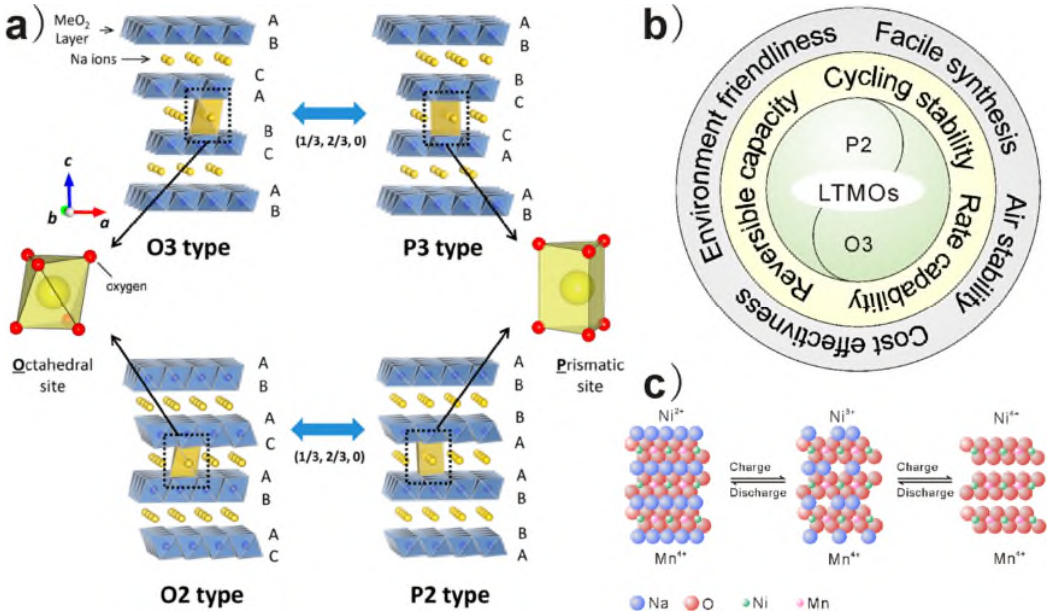

Fig. 1. (a) Classification of P2 and O3 type layered materials with sheets of edge-sharing TMO6 octahedra and related phase transition processes induced by Na^+ extraction. Reproduced with permission.[15] Copyright 2014, American Chemical Society. (b) Overall battery performance of LTMOs cathode material for SIBs. (c) Illustration of the valence evolution of Ni ion and Mn ion during charge/discharge cycling.

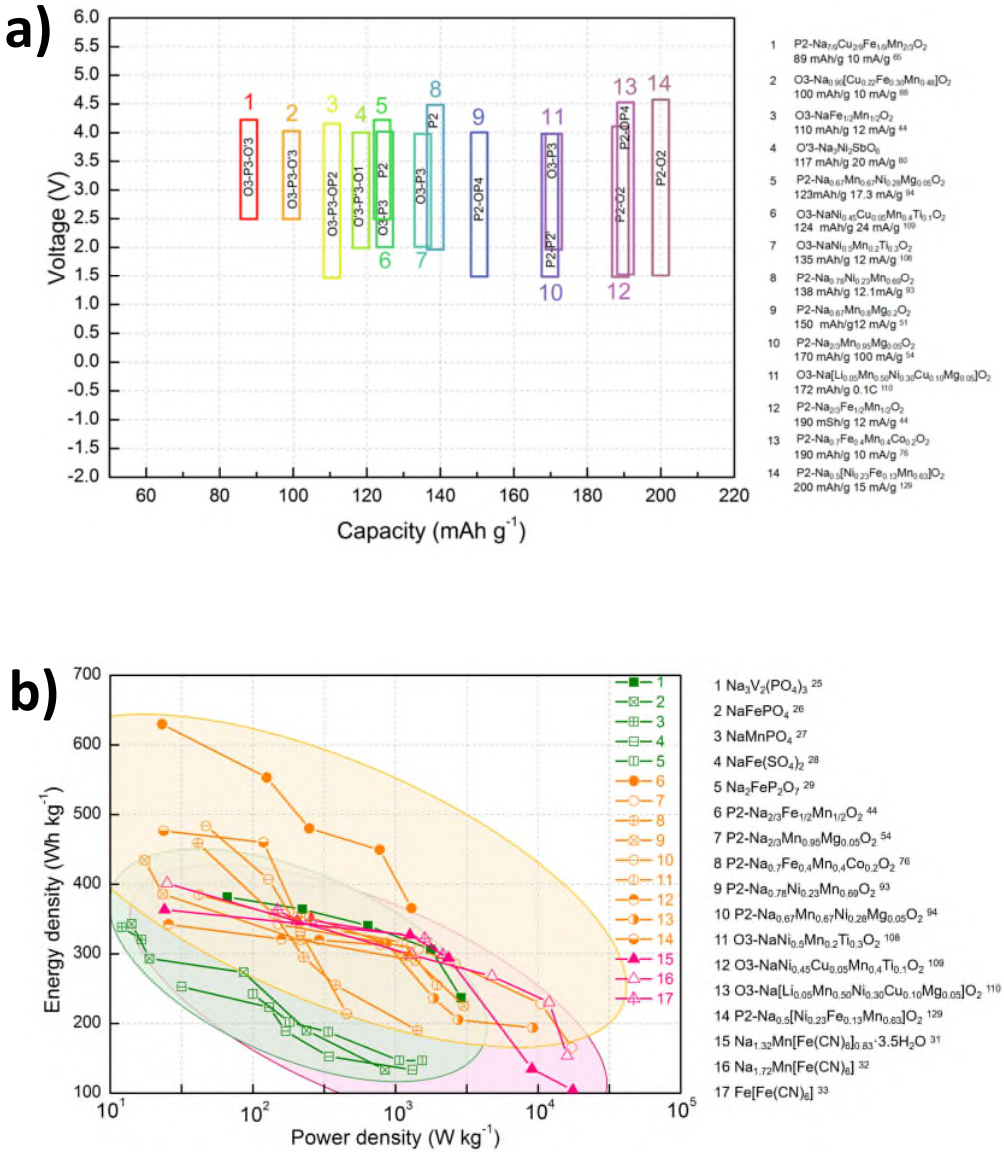

Fig. 2. (a) Comparison of reversible capacity and working voltage ranges of LTMOs with improved battery performance as cathode material for SIB, the related phase transition process are also included. (b) Ragone plots for devies based on Polyanion-Type Compounds(1-5), LTMOs(6-14), PBAs(15-17).

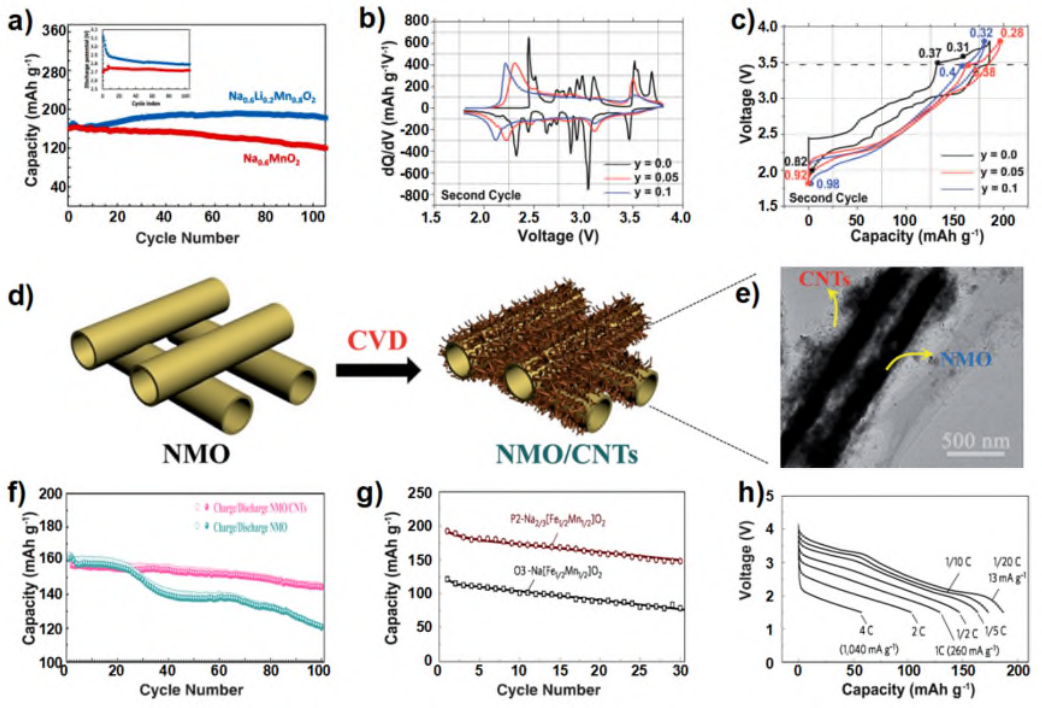

Fig. 3. (a) Electrochemical performance and average discharge potentials (inset) of $Na_{0.6}MnO_2$ (red) and $Na_{0.6}Li_{0.2}Mn_{0.8}O_2$ (blue) cathodes in sodium half-cells at C/15 rate. Reproduced with permission.[49] Copyright 2016, American Chemical Society. (b) Differential capacity vs. voltage plots, and (c) electrochemical profile of the $Na_{2/3}Mn_{1-y}Mg_yO_2$ (y= 0.0, 0.05 and 0.1) composites. The compounds were cycled at 10 mA g^{-1} between 1.8 and 3.8 V vs. Na^+ /Na. Reproduced with permission.[54] Copyright 2016, Royal Society of Chemistry. (d) Schematic illustration of the synthesis of the NMO/CNT composite, (e) TEM image of the NMO/CNT composite, and corresponding (f) cycling performance at 0.1 A g^{-1} NMO and NMO/CNT. Reproduced with permission.[59] Copyright 2016, Royal Society of Chemistry. Comparison of discharge capacity retention (g) and rate capability (h) of P2-$Na_{2/3}[Fe_{1/2}Mn_{1/2}]O_2$ and O3-$Na[Fe_{1/2}Mn_{1/2}]O_2$ based half cell. The cell was charged (oxidized) to 4.2 V at a rate of 13 mA g^{-1} and then discharged (reduced) to 1.5 V at different rates of 1/20 (13 mA g^{-1})-4C (1,040 mA g^{-1}).[44] Copyright 2012, Macmillan Publishers Limited.

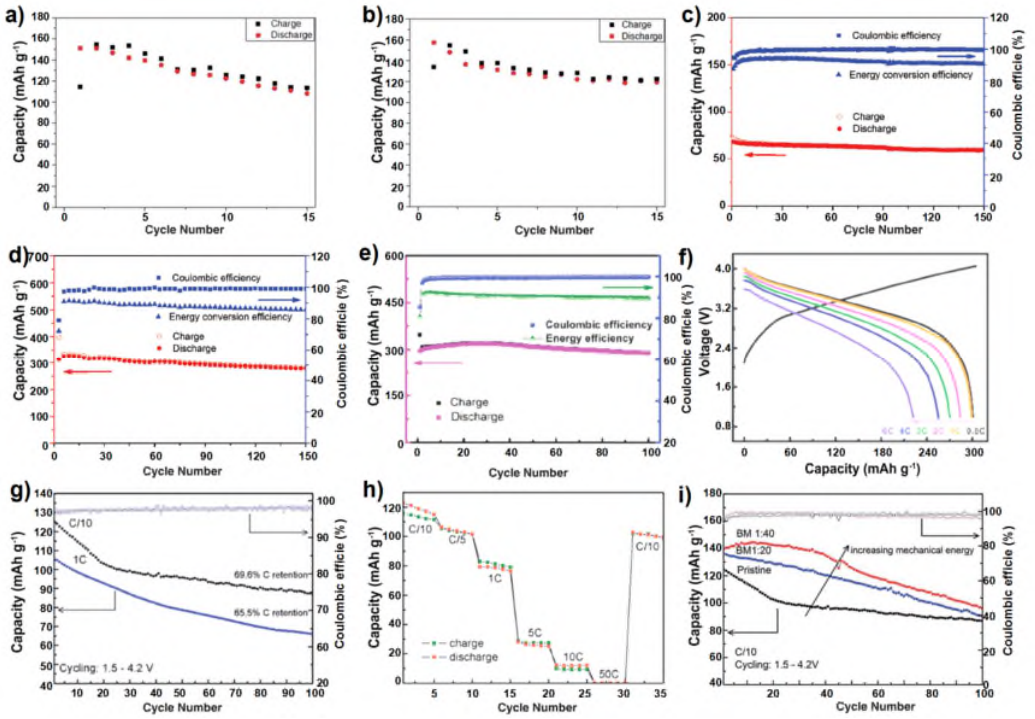

Fig. 4. Cycling stability and capacity obtained for P2- (a) and O3- (b) $Na_{2/3}Fe_{2/3}Mn_{1/3}O_2$ at C/10 rate after 15 cycles. Reproduced with permission.[41] Copyright 2014, Royal Society of Chemistry. (c) Cycling performance of $Na_{7/9}Cu_{2/9}Fe_{1/9}Mn_{2/3}O_2$ electrode at 1 C rate using half-cell, (d) cycling performance of $Na_{7/9}Cu_{2/9}Fe_{1/9}Mn_{2/3}O_2$ electrode at 0.2 C rate using $Na_{7/9}Cu_{2/9}Fe_{1/9}Mn_{2/3}O_2$//hard carbon full cell. Reproduced with permission.[65] Copyright 2015, WILEY-VCH Verlag GmbH & Co. KGaA, Weinheim. Na storage performance of the O3-$Na_{0.9}[Cu_{0.22}Fe_{0.30}Mn_{0.48}]O_2$//hard carbon full cells (e) (f), (e) long-term cycling performance, the Coulombic efficiency, and the energy conversion efficiency versus cycle number at 0.5 C rate and (f) rate capability. Discharge curves of the full cell cycled at constant charge/discharge rates from 0.5C to 6C (one charge curve at 0.5 C rate is also shown). Reproduced with permission.[66] 2015 WILEY-VCH Verlag GmbH & Co. KGaA, Weinheim. (g) Specific discharge capacity (left y axis) and coulombic efficiency (right y axis) *vs.* cycle number for biphasic P2/O3-$Na_{2/3}Li_{0.18}(Mn_{0.8}Fe_{0.2})O_2$ at C/10 rate (black curve) and 1C rate (blue curve), (h) rate capability experiment with charge (green) and discharge (orange) capacity curves, (i) Galvanostatic experiments on pristine and ball milled (BM) samples, performed at C/10 rate and cut-off voltage of 4.2 V vs. Na^+ /Na. Reproduced with permission.[67] Copyright 2018, Royal Society of Chemistry.

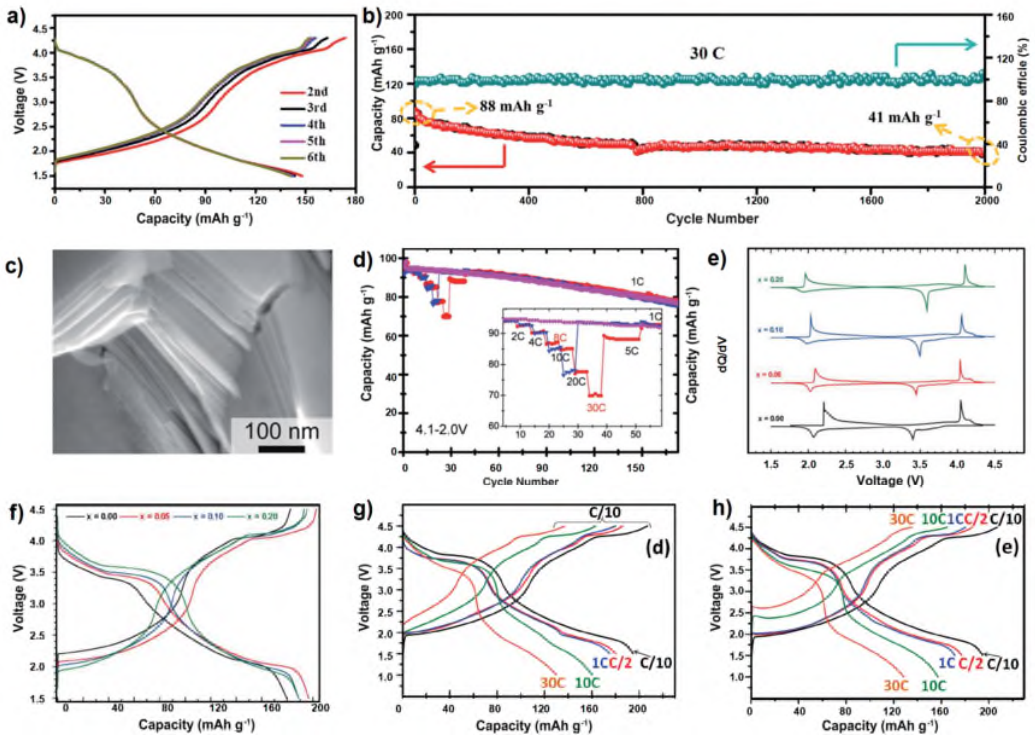

Fig. 5. (a) Charge/discharge profiles of P2-$Na_{0.67}Co_{0.5}Mn_{0.5}O_2$ between 1.5 and 4.3 V at 0.1 C rate, (b) long-term cyclic performance with coulombic efficiency of P2-$Na_{0.67}Co_{0.5}Mn_{0.5}O_2$ for 2000 cycles at 30C. Reproduced with permission.[73] Copyright 2016, Royal Society of Chemistry. (c) SEM images of P2-$Na_xCo_{0.7}Mn_{0.3}O_2$(x≈1.0), (d) specific capacity of Na/P2-$Na_xCo_{0.7}Mn_{0.3}O_2$(x≈1.0) cells as a function of cycle number at 1C for cells with and without prior high current cycling measurement. Reproduced with permission.[75] Copyright 2016, Royal Society of Chemistry. (e) The dQ/dV plots, (f) capacity versus voltage profiles for P2-$Na_{0.7}[(Fe_{0.5}Mn_{0.5})_{1-x}Co_x]O_2$ materials (x=0, 0.05, 0.10, and 0.20). Reproduced with permission.[76] Copyright 2015, WILEY-VCH Verlag GmbH & Co. KGaA, Weinheim. (g) Slow charge and fast discharge mode (applying a charge current rate of C/10 and discharge current rate of C/10 to 30 C) and (h) fast charge and fast discharge mode (applying the same charge and discharge current of C/10 to 30 C) for P2-$Na_{2/3}(Mn_{1/2}Fe_{1/4}Co_{1/4})O_2$. Reproduced with permission.[77] Copyright 2015, WILEY-VCH Verlag GmbH & Co. KGaA, Weinheim.

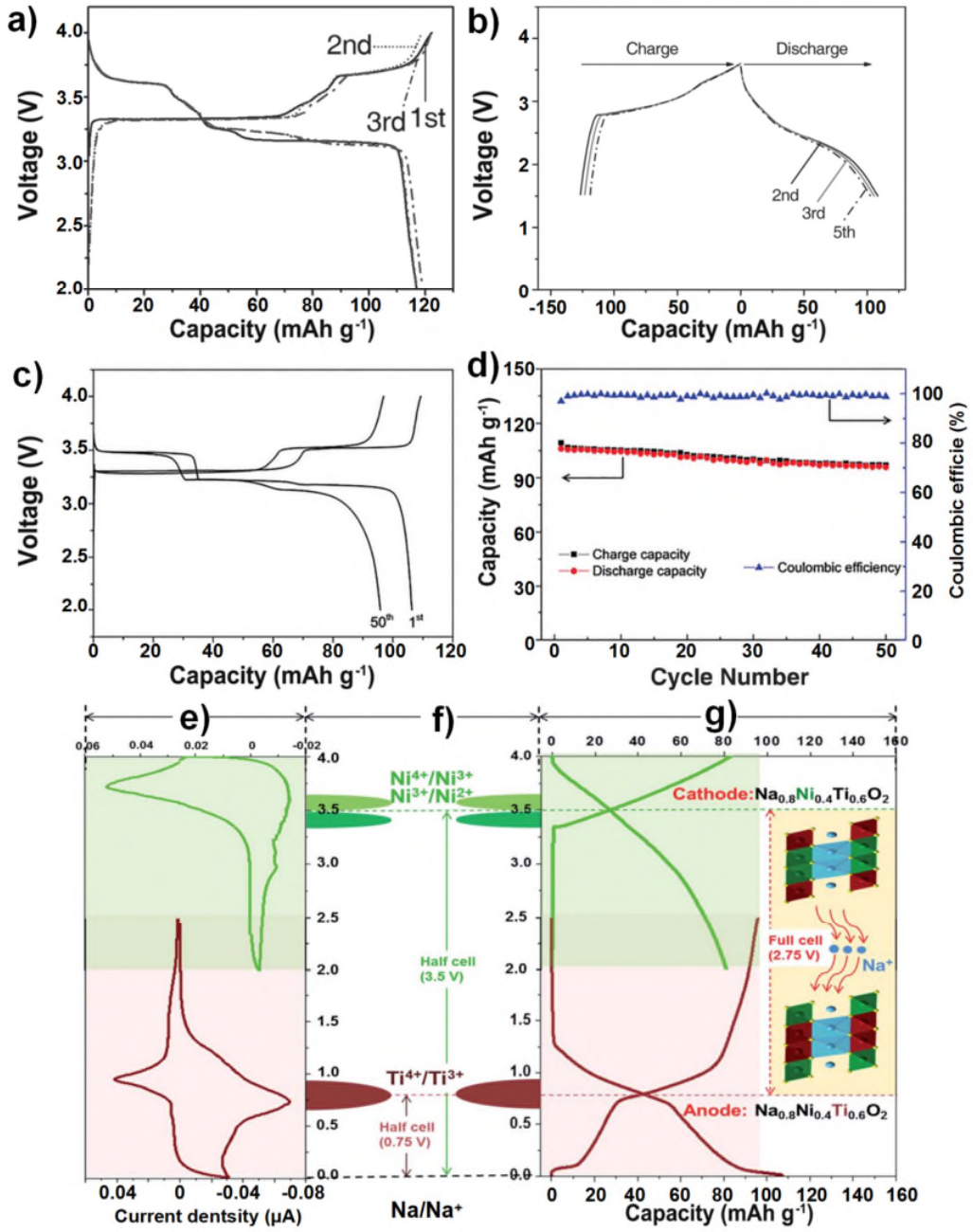

Fig. 6. (a) Galvanostatic charge/discharge (oxidation/reduction) curves for $Na_3Ni_2SbO_6$-based half cells at a rate of 0.1 C (20 mAg^{-1}), (b) charge and discharge profile of $Na_3Ni_2SbO_6$ using a $Na_3Ni_2SbO_6$ cathode and Sb/C anode when cycled at 0.1 C (20 mAg^{-1}). Reproduced with permission.[80] Copyright 2014, WILEY-VCH Verlag GmbH & Co. KGaA, Weinheim.(c) charge-discharge curves of the $Na_3Ni_2BiO_6$ electrode at the 1st and 50th galvanostatic cycles recorded at a rate of 0.05 C, assuming a theoretical capacity of 109 mAh g^{-1}, (d) cycle number

versus capacity at a rate of 0.05C between 2.0 and 4.0 V. Reproduced with permission.[82] Copyright 2017, Royal Society of Chemistry. (e) The CV curves of O3-type $Na_{0.8}Ni_{0.4}Ti_{0.6}O_2$ in the voltage range of 2–4 V for Ni^{4+}/Ni^{2+} (green) and 0.01-2.5 V for Ti^{4+}/Ti^{3+}(brown) vs. Na^+ /Na, (f) schematic of potential of the Ni^{4+}/Ni^{3+}, Ni^{3+}/Ni^{2+} and Ti^{4+}/Ti^{3+} redox couples vs. Na/Na^+ in layered $Na_{0.8}Ni_{0.4}Ti_{0.6}O_2$ materials, (g) the typical charge–discharge profiles of the $Na_{0.8}Ni_{0.4}Ti_{0.6}O_2$/Na half cells in the voltage range of 2–4 V (green) and 0.01–2.5 V (brown) vs. Na^+ /Na. Reproduced with permission.[86] Copyright 2015, Royal Society of Chemistry.

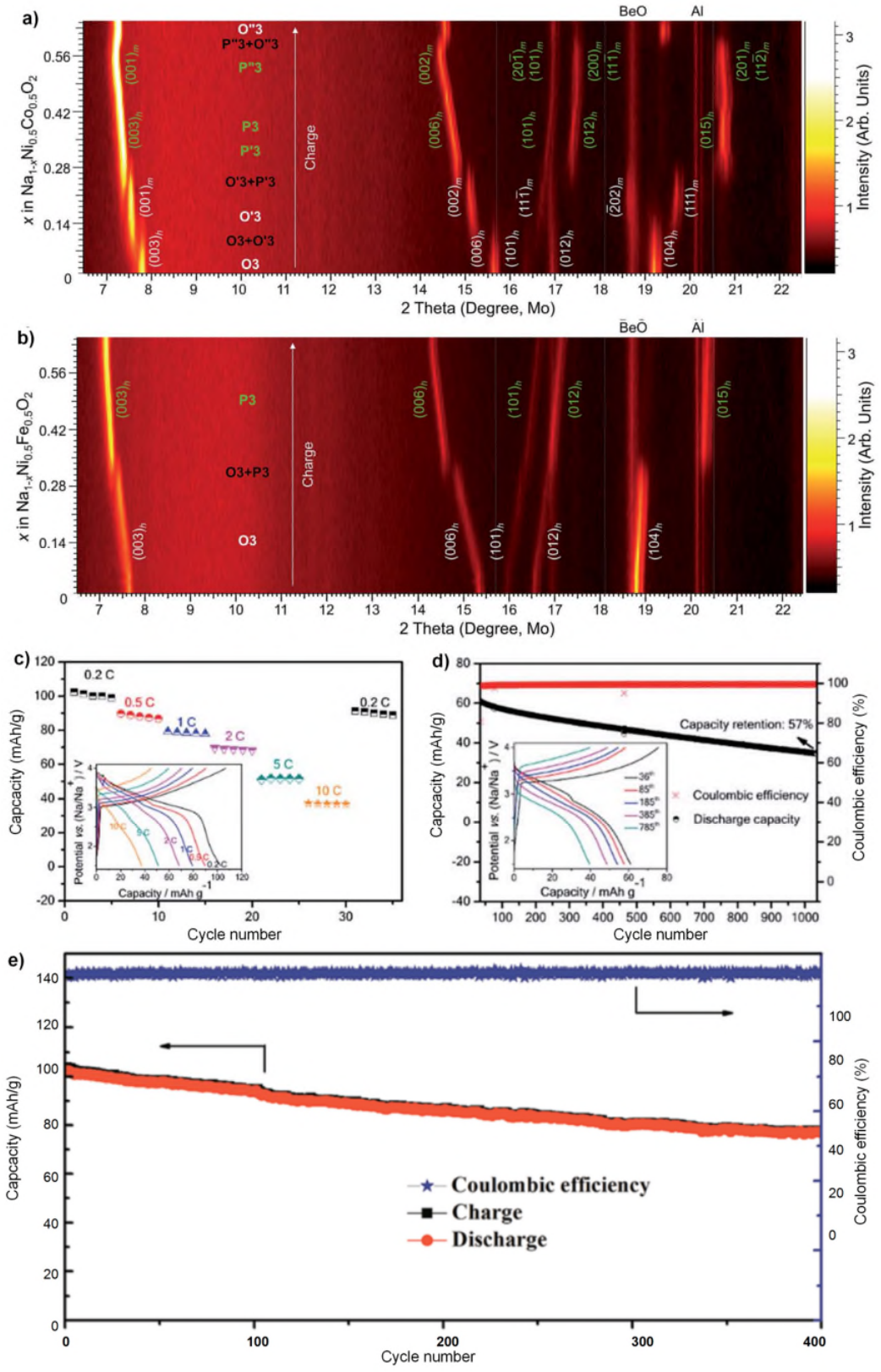

Fig. 7. Intensity contour maps (bird's eye view) of the *in situ* XRD patterns of (a) $NaNi_{0.5}Co_{0.5}O_2$

and (b) $NaNi_{0.5}Fe_{0.5}O_2$ in the 1st charge. Reproduced with permission.[88] Copyright 2017, Royal Society of Chemistry. (c) Discharge capacities of O3-$Na[Fe_{1/3}Ni_{1/3}Ti_{1/3}]O_2$ at various current rates. Inset: the charge/discharge profiles of the first scan for each current rate, (d) cycling behavior of O3-$Na[Fe_{1/3}Ni_{1/3}Ti_{1/3}]O_2$ at 2 C for 1000 cycles after the rate measurement. Inset: the corresponding 36th , 85th , 185th , 385th and 785th charge/discharge profiles. Reproduced with permission.[91] Copyright 2016, Royal Society of Chemistry. (e) Long term cyclic performances of the O3-$NaNi_{1/4}Co_{1/4}Fe_{1/4}Ti_{1/4}O_2$ electrode cycled at a current density 5C. Reproduced with permission.[92] Copyright 2015, Royal Society of Chemistry.

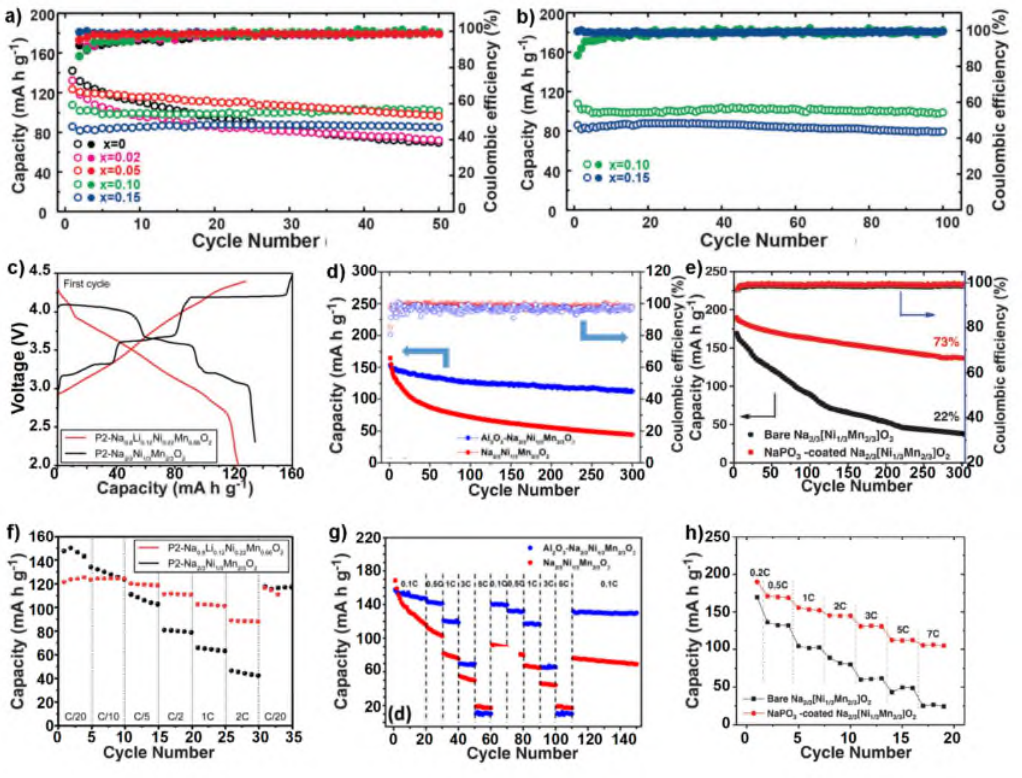

Fig. 8. (a) Cycling performance of various P2-type $Na_{0.67}Mn_{0.67}Ni_{0.33-x}Mg_xO_2$ electrodes (x = 0, 0.02, 0.05, 0.10, and 0.15) during 50 cycles, (b) cycling performance of P2-type $Na_{0.67}Mn_{0.67}Ni_{0.33-x}Mg_xO_2$ electrodes (x = 0.10 and 0.15) during 100 cycles. Reproduced with permission.[94] Copyright 2016, Wiley-VCH Verlag GmbH&Co. KGaA, Weinheim. (c) Electrochemical profiles obtained for the first charge/discharge cycle, and (d) rate performance of P2-$Na_{2/3}Ni_{1/3}Mn_{2/3}O_2$ and Li-substituted P2-$Na_{0.8}Li_{0.12}Ni_{0.22}Mn_{0.66}O_2$ cathode materials. Reproduced with permission.[95] Copyright 2017, Royal Society of Chemistry. (e) Cycling stability and (f) rate performance of the P2-$Na_{2/3}Ni_{1/3}Mn_{2/3}O_2$ and Al_2O_3-P2-$Na_{2/3}Ni_{1/3}Mn_{2/3}O_2$. Reproduced with permission.[102] Copyright 2016, Elsevier Ltd. (g) Cyclability and coulombic efficiency of bare and $NaPO_3$-coated $Na_{2/3}[Ni_{1/3}Mn_{2/3}]O_2$ cathodes combined with hard carbon anode for 300 cycles, and (h) rate capability at various C rates. Reproduced with permission.[104] Copyright 2018, Wiley-VCH Verlag GmbH&Co. KGaA, Weinheim.

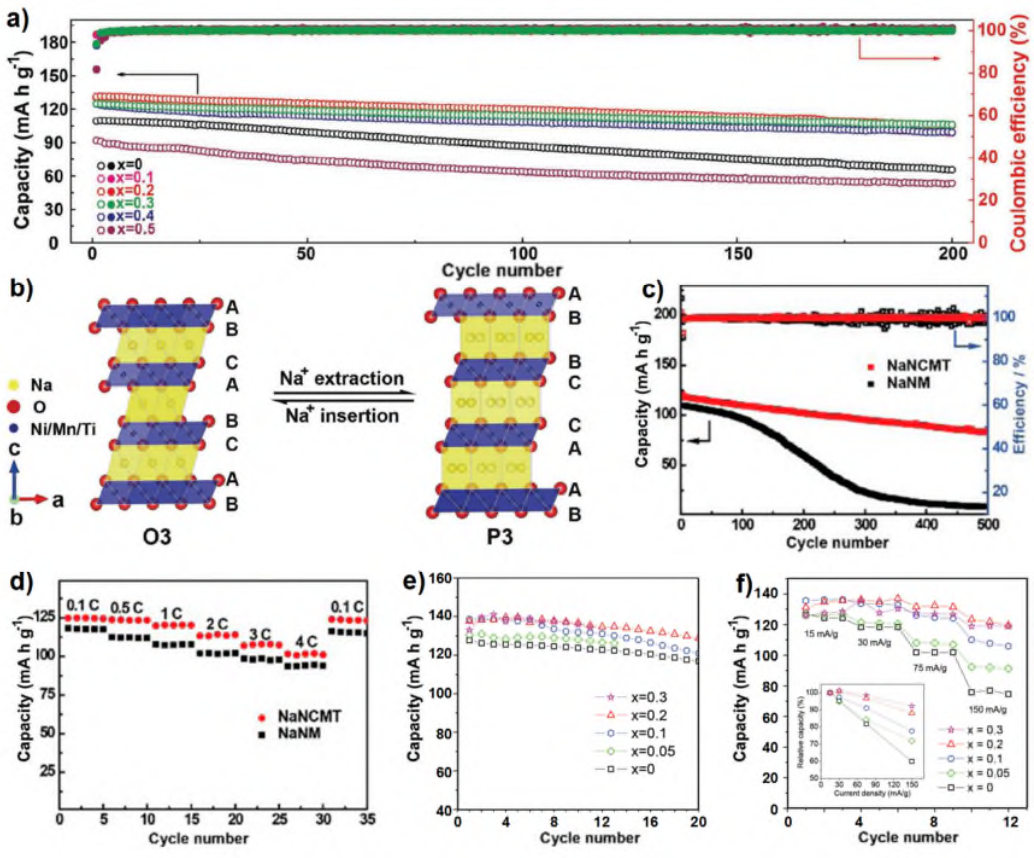

Fig. 9. (a) Cycling performance of various O3-$NaNi_{0.5}Mn_{0.5-x}Ti_xO_2$ electrodes (x = 0, 0.1, 0.2, 0.3, 0.4, and 0.5) during 200 cycles at 1C, (b) schematic illustration showing the O3-P3 phase evolutions during the Na insertion/extraction process. Reproduced with permission.[108] Copyright 2017, Wiley-VCH Verlag GmbH & Co. KGaA, Weinheim. (c) Comparison of cycling stability and Coulombic efficiency tested at 1C and (d) rate performance of $NaNi_{0.5}Mn_{0.5}O_2$ and Cu/Ti co-doped $NaNi_{0.45}Cu_{0.05}Mn_{0.4}Ti_{0.1}O_2$. Reproduced with permission.[109] Copyright 2017, American Chemical Society. (e) Cycle capability and (f) rate performance of $Na_{1-x}Li_xNi_{0.5}Mn_{0.5}O_{2+d}$ ($0 \leq x \leq 0.3$). Inset of (f) shows the relative capacity as a function of applied current density. Reproduced with permission.[111]Copyright 2014, Wiley-VCH Verlag GmbH & Co. KGaA, Weinheim.

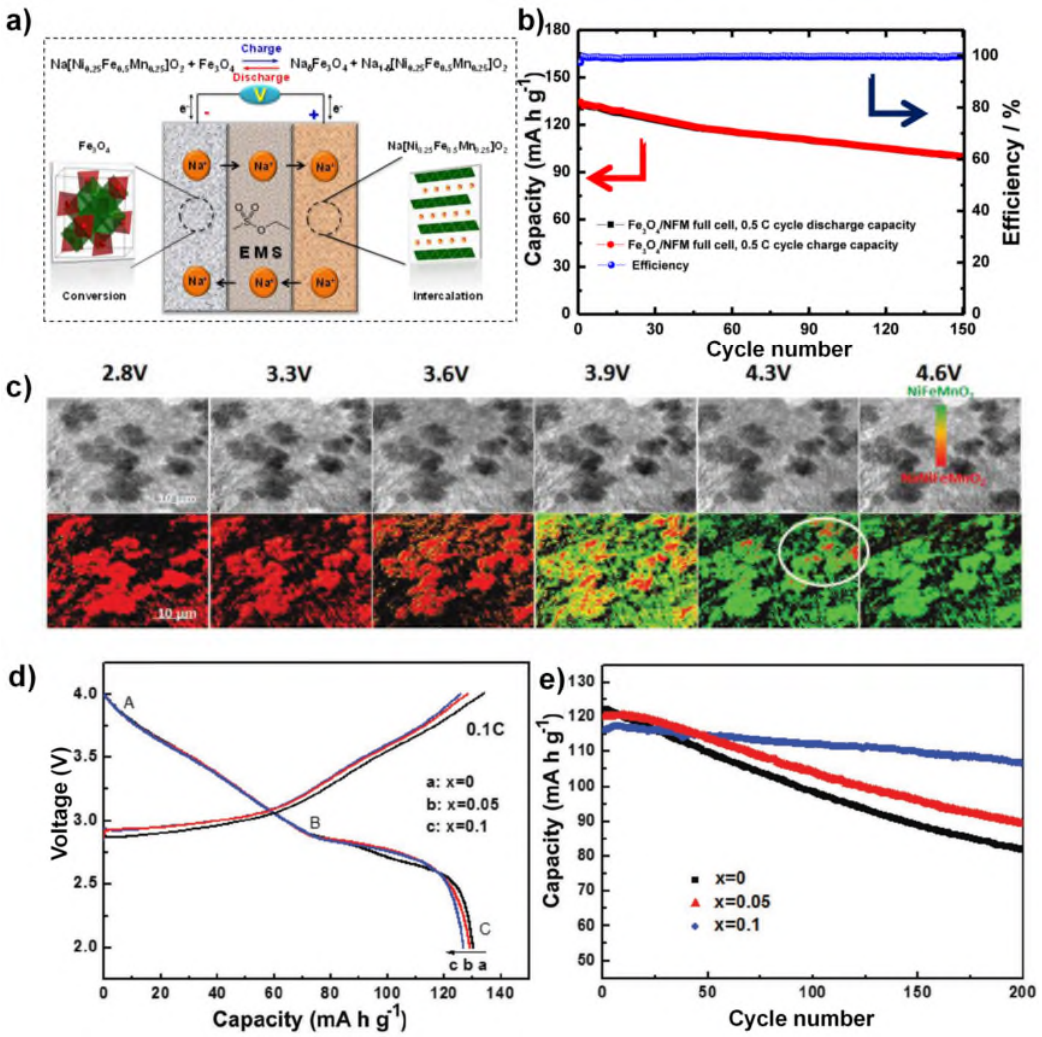

Fig. 10. (a) Scheme of the C-Fe_3O_4/$NaClO_4$-EMS+2 vol% FEC/$Na[Ni_{0.25}Fe_{0.5}Mn_{0.25}]O_2$ full SIB and (b) its cycle performance. Reproduced with permission.[128] Copyright 2014, American Chemical Society. (c) Morphology evolution and chemical phase mappings of $NaNi_{1/3}Fe_{1/3}Mn_{1/3}O_2$ using in operando TEM imaging approach during denatrium reaction. Reproduced with permission.[131] Copyright 2016, Wiley-VCH Verlag GmbH & Co. KGaA, Weinheim. Comparison of the first charge/discharge profiles of O3-$Na_{1-x}Ca_{x/2}Ni_{1/3}Fe_{1/3}Mn_{1/3}O_2$ (x = 0, 0.05, 0.10) samples at 0.1C rate (d) and the cycling performance of the O3-$Na_{1-x}Ca_{x/2}Ni_{1/3}Fe_{1/3}Mn_{1/3}O_2$ (x = 0, 0.05, 0.10) electrodes at 1C rate (e). Reproduced with permission.[132] Copyright 2018, Wiley-VCH Verlag GmbH & Co. KGaA, Weinheim